IMPACT OF CATTANEO-CHRISTOV DOUBLE DIFFUSION ON A SUTTERBY NANOFLUID FLOW OVER A ROTATING DISK WITH HALL CURRENT AND ION SLIP

STUDENT NAME: ASAD ALI SHAH
ENROLLMENT NO: 01-248202-001
SUPERVISOR BY PROF. DR. MUHAMMAD RAMZAN

A thesis submitted in fulfilment of the requirements for the awardof degree of
Masters of Science (Mathematics)

Department of Computer Science

BAHRIA UNIVERSITY ISLAMABAD

Session (2020-2022)

Approval of Examination

Scholar Name: AsadAli Shah

Registration Number: 35286

Enrollment: 01-248202-001

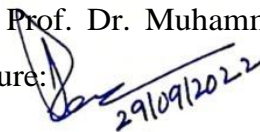Program of Study: MS (Mathematics)

Thesis Title: Impact of Cattaneo-Christov double diffusion on a Sutterby nanofluid flow over a rotating disk with Hall current and Ion slip

It is to certify that the above scholar's thesis has been completed to my satisfaction and, to my belief, its standard is appropriate for submission for examination. I have also conducted plagiarism test of this thesis using HEC prescribed software and found similarity index 17% that is within the permissible limit set by the HEC for the MS/M. Phil degree thesis. I have also found the thesis in a format recognized by the BU for the MS/M. Phil thesis.

Supervisor Name: Prof. Dr. Muhammad Ramzan

Supervisor Signature: 29/09/2022

Date:

Author's Declaration

I, Asad Ali Shah hereby state that my MS/MPhil thesis titled "Impact of Cattaneo-Christov double diffusion on a Sutterby nanofluid flow over a rotating disk with Hallcurrent and Ion slip" is my own work and has not been submitted previously byme for taking any degree from this university Bahria University or anywhere else inthe country/world. At any time if my statement is found to be incorrect even after my Graduate the university has the right to withdraw/cancel my MS/MPhil degree

Name of Scholar: ASAD ALI SHAH

Date: 2 9 /9/2022

Plagiarism Undertaking

I, solemnly declare that research work presented in the thesis titled "Impact of Cattaneo-Christov double diffusion on a Sutterby nanofluid flow over a rotating disk with Hall current and Ion slip" is solely my research work with no significant contribution from any other person. Small contribution/help wherever taken has been duly acknowledged and that complete thesis has been written by me.

I understand the zero tolerance policy of the HEC and Bahria University towards plagiarism. Therefore, I as an Author of the above titled thesis declare that no portion of my thesis has been plagiarized and any material used as reference is properly referred/cited.

I undertake that if I am found guilty of any formal plagiarism in the above titled thesis even after award of MS/MPhil degree, the university reserves the right to withdraw/revoke my MS/MPhil degree and that HEC and the University has the right to publish my name on the HEC/University website on which names of students are placed who submitted plagiarized thesis.

Name of Scholar: Asad Ali Shah

Date: 29/09/2022

Dedication

My beloved parents, sister, wife, children, colleagues and respected teachers.Thanks for your love, prayers and support.

Acknowledgements

Abstract

Classical Fourier law has been a benchmark for about two centuries. But owing to serious flaws, this was later amended and now-a-days is termed as Catteneo-Christov heat flux model. This thesis discusses the flow of Sutterby nanofluid flow over a rotating disk with Catteneo-Christov double diffusion. The whole system is influenced by Hall current and Ion slip. The stability of the nanofluid is enhanced by considering gyrotactic microorganisms. The problem is solved numerically by engaging bvp4c the built-in function of MATLAB software. The outcomes are depicted via graphical illustrations. The reliant results show that fluid velocity is influenced by Hall current and Ion slip. Moreover, a drop in microorganism profile is seen for bioconvection Lewis number.

TABLES OF CONTENTS

LIST OF TABLES

LIST OF FIGURES

NOMENCLATURE

(u, v, w)	Components velocity along (r, θ, z)
f , g	Non-dimensional stream functions
K	Material parameter of Riener-Rivlin fluid
b	Stretching Rate
D_T	Thermophoretic diffusion coefficient
D_B	Brownian diffusion coefficient
B_0	Magnetic field strength
p	Pressure
β_i	Hall slip parameter
β_e	Ion slip parameter
N_b	Brownian motion parameter
T	Temperature
M	Magnetic parameter
N	Microorganisms density
ρ	Density
μ	Dynamic viscosity
Le	Lewis number
T_w	Temperature at the surface of the disk
T_∞	Ambient temperature
Pe	Peclet number
Pr	Prandtl number
τ_{ij}	Component of Shear stress
C_w	Concentration near the disk's surface

C_∞	Ambient concentration
τ	Capacity ratio or heat capacity of solid particles and nanofluid
$k(\mathrm{T})$	Variable thermal conductivity
c_p	Specific heat
S_c	Schmidt number
N_t	Thermophoretic parameter
v	Kinematic viscosity
D_n	Microorganism's diffusivity
τ_w	Shear stress
ϵ_1	Material parameter
α_1, β_1	Radial slip coefficients
α_2, β_2	Azimuthal slip coefficients
α, β_3	Thermal slip coefficients
γ, β_4	Concentration slip coefficients
α_m	Thermal diffusivity
k	Thermal conductivity
$(\rho c)_p$	Capacity of nano particles
$(\rho c)_f$	Heat capacity of the base fluid
S_c	Schmidt number
σ	Electrical conductivity
λ_e	Heat diffusion relaxation time
λ_c	Mass flux relaxation time
α^*	Stretching parameter

Chapter 1

Preliminaries

1.1 Fluid

Fluid is a substance that reshapes constantly under the external influence or imposed shear stress. Liquids, gases, and plasma are all examples of fluids.

1.2 Nanofluid and base fluid

A nanofluid is a colloidal solution of nanoparticles made up of nanometer-sized particles floating in a base fluid. With water, ethylene glycol, and oil serving as the primary fluids, metals, oxides, carbides, and carbon nanotubes are frequently used as nanoparticles in nanofluids. Nanoparticles are used to increase the thermal conductivity of the fluid.

1.3 Hybrid nanofluid flow

Adding one or more than one nanoparticle to the basic fluid, is terms as "hybrid nanofluid", may improve the thermal characteristics of the nanofluid. A hybrid nanofluid is a high-tech fluid that contains several nanoparticles that can boost heat transfer rates.

1.4 Fluid mechanics

The study of fluids in motion and at rest is known as fluid mechanics. It is classified into the following two subcategories:

1.4.1 Fluid statics

It is a sub-discipline that studies the properties of liquids in a stationary condition.

1.4.2 Fluid dynamics

It is a sub-discipline that studies the properties of liquids in motion.

1.5 Stress

The ratio of applied force (F) to cross-section area (A) is used to define stress. In a symbolic sense, we have

$$Stress = \frac{F}{A}. \tag{1.1}$$

The unit of stress in the SI system is $\frac{Kg}{m\ s^2}$ and the dimension is $ML^{-1}T^{-2}$. It is further divided into two types.

1.5.1 Shear stress

Shear stress is the type of stress that occurs when an external force operates parallel to the surface unit area.

1.5.2 Normal stress

When a force applied vertically on the surface of a unit area, it is referred to as normal stress.

1.5.3 Strain

Strain is a dimensionless quantity that is used to quantify an object's deformation when a force is applied to it.

1.6 Flow

Flow is defined as a substance that deforms smoothly and uniformly when subjected to diverse forces. The following are the two primary subcategories of flow:

1.6.1 Laminar flow

The fluid moves along regular lines with no interruption between the layers, resulting in laminar flow.

1.6.2 Turbulent flow

When the velocity of the fluid particles in the flow field is irregular, turbulence occurs.

1.7 Viscosity

The viscosity of a fluid is a fundamental feature that determines resistant to flow when many forces are operating on it. The following is a mathematical representation:

$$\text{viscosity} = \frac{\text{shear stress}}{\text{gradient of velocity}}. \tag{1.2}$$

1.7.1 Dynamic viscosity

The measure of internal resistance to flow is dynamic viscosity (μ), often known as absolute viscosity. It has $M\ L^{-1}T^{-1}$ as a dimension. Kinematic viscosity (ν) the ratio of viscosity (μ) to fluid density (ρ) is known as kinematic viscosity. It is expressed

mathematically by,

$$\nu = \frac{\mu}{\rho}.$$ (1.3)

1.8 Classification of fluid

1.8.1 Inviscid fluid

Ideal fluid, often known as inviscid fluid, is a fluid with no viscosity.

1.8.2 Real fluid

Real fluid is defined as a fluid with a viscosity that is not zero. There are two types of fluid in this category:

1.8.3 Newtonian fluids

These are fluids that comply with Newton law of viscosity and have a constant viscosity. The shear force τ_{yx} is directly proportional to the velocity gradient $\left(\frac{du}{dy}\right)$ in these fluids. Newtonian fluids include alcohol, water, glycerine, and kerosene.

$$\tau_{yx} = \mu \frac{du}{dy}.$$ (1.4)

Here the shear stress (τ_{yx}), viscosity (μ) and deformation rate $\left(\frac{du}{dy}\right)$ respectively.

1.8.4 Non-Newtonian fluids

These are the fluids that do not follow Newton viscosity law. Shear stress τ_{yx} and velocity gradient have a nonlinear relation.

$$\tau_{yx} = k \left(\frac{du}{dy}\right)^n,$$ (1.5)

for $n \neq 1$, where the consistency(k) and behavior index (n) respectively.

1.8.5   Compressible fluid

When the density of a fluid varies with temperature and pressure, it is referred to as a compressible fluid. Gases are one of the most common examples.

1.8.6   Incompressible fluid

Incompressible fluid is defined as a fluid whose density is independent of temperature and pressure. Liquids are often thought to be incompressible.

1.9   Boundary layer

The viscosity of the fluid is prominent at the layer near to fluid surface. In general, the boundary layer is the zone where viscosity has the most influence.

1.10   Heat and mass transfer

Heat transfer is a kinetic process in which energy is transferred from one particle to another. Mass transfer, on the other hand, is the movement of mass from one location to another, such as by absorption or evaporation. As a result, the efficiency of these two operations is regarded as a whole.

1.11   Density

The density of a substance is its mass (m) per unit volume (V). This measurement is used to determine how much matter is contained in a given volume. The following is a mathematical expression:

$$\rho = \frac{m}{V}.\tag{1.6}$$

1.12 Pressure

The force (F) applied to a surface per unit area (A) is known as pressure. SI unit of pressure is $\frac{N}{m^2}$.

$$P = \frac{F}{A}. \tag{1.7}$$

1.13 Heat transmission mechanism

Heat is the energy that travels from a warmer to a colder location. The heat transfer phenomena occurs when two objects at different temperatures come into contact. Heat is dispersed by three basic mechanisms: conduction, convection, and radiation.

1.14 Conduction

By colliding free electrons and molecules, heat is transported from a heated area to a cold area of liquids and solids. Molecules are not transported in this event.

$$\boldsymbol{q} = -k\frac{dT}{dx}, \tag{1.8}$$

where Heat flux density $(\boldsymbol{q})$, Material's conductivity (k) and Temperature gradient $\left(\frac{dT}{dx}\right)$.

1.15 Convection

Due to the mobility of molecules, heat is transferred from a hot region to a region of liquids and gases in this process.

$$Q = hA\Delta T, \tag{1.9}$$

where Heat transfer rate (Q), Convection heat-transfer coefficient (h), Exposed surface area (A) and Temperature difference (ΔT).

1.16　Radiation

Radiation is a technique through which heat is transported by electromagnetic waves. When heat is transported through a vacuum, this process is critical.

$$q = e\sigma A \left(\Delta T\right)^4,\tag{1.10}$$

where Heat transfer (q), Emissivity of the system (e), Stephen-Boltzmann constant (σ), Area (A) and Temperature difference between two systems (ΔT).

1.17　Dimensionless numbers

1.17.1　Prandtl number

It's a non-dimensional number that represents a change in kinematic viscosity (ν) in relation to thermal diffusivity. Mathematically,

$$Pr = \frac{\nu}{\alpha},\tag{1.11}$$

where viscous diffusion rate (ν), thermal diffusion rate (α).

1.17.2　Reynolds number

The non-dimensional number that describes the transition from inertial to viscous forces. Mathematically

$$Re = \frac{\rho V D}{\mu},\tag{1.12}$$

where Fluid density (ρ), Fluid velocity (V), Diameter (D), Fluid viscosity (μ).

1.17.3 Brownian motion parameter

Brownian motion occurs in a nanofluid owing to the size of the nanoparticles. It's a nanoscale mechanism that demonstrates nanofluid's thermal effects. Mathematically,

$$N_b = \frac{\tau D_B \left(C_f - C_\infty\right)}{\nu},$$ (1.13)

where, the ratio of effective heat and heat capacity of the nanoparticles and fluid respectively (τ), wall's concentration (C_f), ambient concertration (C_∞), kinematic viscosity (ν), brownian diffusion coefficient (D_B).

1.17.4 Thermophoresis parameter

Thermophoresis is a process that prevents different particles from combining owing to a pressure differential as they travel together or separates a mixture of particles after it has been mixed together. Thermophoresis is positive on a cold surface and negative on a hot surface.

$$N_t = \frac{\tau D_T \left(T_f - T_\infty\right)}{\nu T_\infty},$$ (1.14)

where, the ratio of effective heat and heat capacity of the nanoparticles and fluid respectively (τ), wall's temperature (T_f), ambient concertration (T_∞), kinematic viscosity (ν), thermophoretic coefficient (D_T).

1.18 Fundamental laws

1.18.1 Mass conservation law

It says that the overall mass of any closed system will stay constant. Mathematically

$$\frac{Dp}{Dt} + \rho \nabla . V = 0,$$ (1.15)

If the fluid is incompressible, then the equation above applies.

$$\nabla .V = 0. \tag{1.16}$$

1.18.2 Momentum conservation law

The total linear momentum is constant for closed system, according to the law of conservation of momentum. In most cases, it is represented as:

$$\rho \frac{DV}{Dt} = \text{div } \tau + \rho b, \tag{1.17}$$

where Cauchy stress tensor (τ) and Body force (b).

1.18.3 Energy conservation law

The energy equation, generally known as the energy conservation law is given by:

$$\rho \frac{De}{Dt} = \tau .L + \rho r - \nabla .\boldsymbol{q}, \tag{1.18}$$

where specific internal energy (e), heat flux $(\boldsymbol{q})$ and Thermal radiation (r). Without thermal radiation, the energy equation is as follows:

$$\rho C_p \frac{DT}{Dt} = \tau .L + k \ \nabla^2 T, \tag{1.19}$$

with $e = C_p T$, $\boldsymbol{q} = k\nabla T$, signifies thermal conductivity (k), while temperature (T).

1.18.4 Thermal diffusivity

The unstable conductive heat flow is described by thermal diffusivity, a material-specific feature. This number shows how quickly a material reacts to temperature changes. It's

the product of thermal conductivity and density, divided by thermal conductivity.

$$\alpha = \frac{k}{\rho C_p},$$ (1.20)

where thermal conductivity (k), specific heat capacity (C_p) and density (ρ).

1.18.5 Thermal conductivity

Thermal conductivity determines a material's capacity to conduct heat. The quantity of heat transfer rate (Q) through a material of unit thickness (L) times unit cross section area (A) and unit temperature difference (ΔT) is given by the heat conduction law of Fourier Law.

$$k = \frac{QL}{A\Delta T} \qquad \left(\text{SI unit is } \frac{W}{mK} \right).$$ (1.21)

1.18.6 Hall current and Ion slip

Hall currents create a three-dimensional field structure and boost the pace of reconnection (growth). The Hall current effect would have an observational significance since the magnetic reversal layer widths in the magnetopause and magnetotail are predicted to become as thin as the Ion inertial length when the reconnection process is anticipated to occur. The effect is amplified in a semiconductor due to the existence of Halls, which are moving positive charge carriers.

$$F_m = eV_dB,$$ (1.22)

where charge drift velocity (V_d), charge of electron (e) and magnetic field strength (B).

1.18.7 Sutterby fluid

The Sutterby fluid extra stress tensor (τ) is written as:

$$\tau = -pI + \acute{S}.$$ (1.23)

The liquid viscosity of Sutterby is shown as:

$$\acute{S} = \mu_0 \left(\frac{\sin^{-1}(b\Phi)}{b\Phi} \right)^n.$$ (1.24)

By using Maclaurin series $sin^{-1}x = x + \frac{1}{3!}x^3 + ...$ and the Binomial theorem $(a+b)^n = a^n + nab^{n-1} + ..$ to expand Equation (2.24) The typical time (b), shear rate viscosity weaker (μ_0), the shear rate (Φ), and the constraint (n) that is dimensionless. By changing $n = 0$ for a viscous model, this model may be obtained. The binomial equation for $n = 1$ is transformed to,

$$\acute{S} \approx \mu_0 \left(1 - \frac{(b\Phi)^2}{6} \right)^n \approx \mu_0 \left(1 - \frac{n(b\Phi)^2}{6} \right).$$ (1.25)

The following is how the shear rate is reported:

$$\Phi = \sqrt{\frac{1}{2}trace(A_1^2)}.$$ (1.26)

The first Rivlin-Erickson tensor is represented as $A_1 = L^t + L$.

Chapter 2

Introduction and literature review

Due to many real-world applications in the fields of aeronautical science and other engineering disciplines, the heat transport problem across a rotating disk continues to get significant attention owing its interesting application, for instance, thermal-power producing systems, rotating machinery, medical gear, computer storage, gas turbine rotors, air purifiers, electronics, and crystal growth procedures. As a result, unlike the classical Von Karman flow with a regular Newtonian fluid.

Nanofluids have shown some amazing uses in different fields of research, including chemical and biomechanics, thermal engineering, industrial technology and nuclear industries. Water and ethylene glycol are conventional base fluids and thermal conductivity of these fluids is very poor so to enhance the thermal conductivity of these fluids we add some nanoparticles in these base fluids and the volume concentration of these nanoparticles should be less than one percent. Choi and Eastman [1] were the first to use the term nanofluids, with the purpose of increasing the thermal conductivity of base liquids. The major focus of his research is on how thermal conductivity is increased, and it is demonstrated by researchers via several exploratory and numerical studies. Fetecau et al. [2] used an isothermal moving surface to study the natural convection flow of a nanofluid. Bhatti and Rashidi [3] anticipated Brownian motion and thermophoresis effects for Williamson flow of nanofluid generated by the stretched structure. The in-

novative work of Turkyilmazoglu [4] reveals nanofluid interaction in a flowing jet. The usage of Bingham nanofluids by cylindrical rings generated by a rotating inner cylinder was examined by Venthan et al. [5]. Waqas et al. [6] looked at nanofluid analysis for Maxwell-based Micropolar with slip effects and porous media. Ali et al. [7] used cross nanofluids and magnetic force to heat transfer a contracting and expanding cylinder.

Non-Newtonian fluid analysis is a topic of interest for scientists and academicians. Examples of non-Newtonian fluids include paints, paper pulp, ketchup, shampoo, and polymer solutions. In contrast to Newtonian fluids, non-Newtonian fluids cannot be described by a single constitutive relation due to their various complexities. As a result, researchers have proposed several mathematical models of non-Newtonian fluids in the past. The couple stress fluid model is one of the viscoelastic fluid model that has been proposed to illustrate non-Newtonian fluid characteristics and behavior. Couple stresses and body couples are included in the couples stress fluid model, which is an extension of the classical fluid model, *i.e.*, the viscous fluid. Examples of few stress fluids are liquid crystals, animal and human blood, colloidal fluids, and liquids with long chain molecules. The notion of the couple stress fluid was first introduced by Stokes [8]. This attempt was followed by another research by Stokes [9], who discussed a couple stress fluid flow past a hydromagnetic channel in chronological sequence. Then, Nguen [10] discovered couple stress fluid boundary layer equations. Soundalgekar [11] investigated solute dispersion between two parallel plates under less pressure. The pulsatile flow of the couple stress fluid past a circular tube was developed by Chaturani and Upadhya [12]. As an application to blood flow problem, Sagayamary and Devanathan [13] discussed the flow of couple stress fluid across a slowly shifting cross channel. The oscillatory movement of the couple stress fluid via a porous material elaborated by Hiremath and Patil [14]. References [15-17] provide more information on couple stress fluid.

The Sutterby fluid model [18] is a dual nature model that takes into consideration of both pseudoplastic and dilatant material properties. By raising the Sutterby fluid parameter, they were able to increase the friction factor at the surface. Hayat et al.

16

[19] looked at the peristaltic transition of the Sutterby fluid while considering entropy minimization in the system. An increase in the material parameter of the Sutterby fluid resulted in a decrease in velocity. References [20-22] provide more information on the Sutterby fluid.

The physical phenomena of wall-driven fully-developed flow in the Buongiorno nanofluid mode. In the instance of nanofluid flow, Buongiorno [23] suggested the several slip structure and proposed that just two major elements, namely thermophoresis and Brownian diffusion, are important in the heat transmission process. Von Kármán [24] simplified the governing complete system of equations for the solution appearing in the spinning disk issue in his pioneering work. Millsaps and Pohlhausen [25] looked at the heat transfer mechanism's spinning disk issue. Shevchuk and Buschmann [26] investigated heat transfer in viscous fluid rotating disk flow and presented the perfect solution.

Bacteria and microalgae have a high density as compared to water, and as a result, they flow in the opposite direction of gravity. Because of this occurrence, the top layer thickens more than the bottom layer, resulting in an unbalanced density distribution. Owing to the convective instability in this scenario, convective patterns arise, according to the physics of the problem. Bioconvection is the word for the random instantaneous pattern activity of microorganisms. References [27-31] geotactic, gyrotactic, chemotactic and bioconvection are the four types. Because of the variability in the nature of such fluids, a generic model is insufficient for accurate simulation.

Heat transport phenomena are crucial from in engineering and industrial applications. Power generating, petroleum refineries, space heating contact, petrochemical facilities, chemical plants, nuclear reactor cooling stations, energy production, and electronic device cooling are only few of the heat transfer uses. Fourier [32] created the law of heat conduction to study heat transmission characteristics. Furthermore, when the disk is rough or has impurities on its surface, achieving no-slip at the disk might be difficult. The partial slip conditions can be used to approximate the no-slip requirement in this case. Despite the aforementioned uses, there is little research on the management of

partial slip situations in non-Newtonian fluid flows. Esfahani and Bordbar [33], used numerical simulation to study laminar double-diffusive natural convection heat transfer increase in a square enclosure filled with different nanofluids. References [34-41] provide recent instances fousing heat transmission.

In order to perform a quantitative examination of the flow, the Hall current and Ion slip relations in Ohms law were ignored. However, in the presence of a strong magnetic field, the effect of Hall current and Ion slip is critical. As a result, the influence of Hall current and Ion slip components of the magneto-hydrodynamics expressions must be taken into account in a variety of real situations. Prasad et al. [42] investigated the Hall characteristics for a stream flowing over a surface with varying thicknesses. Tani [43] investigated the effects of the Hall term on the constant flow of an electrically conducting nanofluid in 1962. The effects of Ion slip, Hall current, and nonlinear radiation on the flow of nanofluids in a channel were reported by Hayat et al. [44]. The effect of Ion-slip and Hall parameters on the flow of nanofluids between two tubes was investigated by Srinivasacharya and Shafeeurrahmann [45]. Furthermore, some recent connected research might be expected in the references [46-55].

Chapter 3

Numerical Study for slip flow of Reiner-Rivlin nanofluid due to a rotating disk

Here we consider non-Newtonian Reiner-Rivlin fluid over a rotating disk with various slip conditions. The thermophoreis and brownian motion effects are disussed using buongiorno model. Similarity transformation are used to convert partial differential equations into ordinary differential equations. Graphs are drawn for various parameter and engineering quantities are overall tabulated.
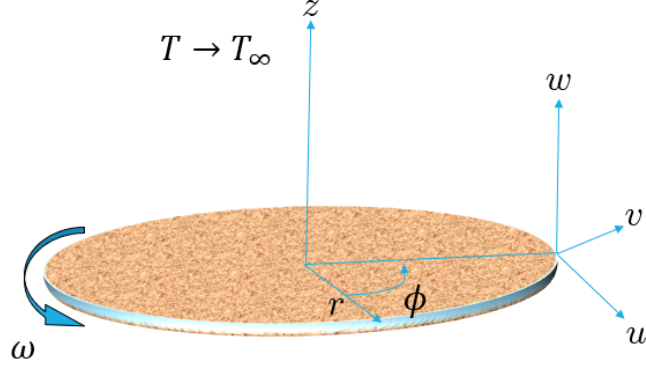
3.1 Mathematical formulation

Figure 3.1 Fluid flow geometry

This research looks at, the Reiner-Rivlin nanofluid flow across a rotating disk with multiple slip effects. The disk is rotating around the vertical axis at a fixed angular velocity ω, generating a swirl in the fluid layers around it. The velocity throughout the directions of r, ϕ and z are u, v and w respectively. Because the boundary layer thickness exceeds the normal scale, concentration, temperature and velocity conditions are employed. The current investigation used the temperature fluctuation condition. Reiner [56] and Rivlin [57] have derived the following relationship, which is an extension of Tabassum and Mustafa [58] work:

$$\tau_{ij} = -p\delta_{ij} + \mu e_{ij} + \mu_c e_{ik} e_{kj} \; ; \; e_{jj} = 0, \tag{3.1}$$

where stress tensor (τ_{ij}), pressure (p), cross-viscosity coefficient (μ_{ij}), Kronecker symbol (δ_{ij}), and deformation rate tensor (e_{ij}).

$$\frac{\partial u}{\partial r} + \frac{\partial w}{\partial z} + \frac{u}{r} = 0, \tag{3.2}$$

$$\rho\left(u\frac{\partial u}{\partial r} + w\frac{\partial u}{\partial z} - \frac{v^2}{r}\right) = \frac{\partial \tau_{rr}}{\partial r} + \frac{\partial \tau_{rz}}{\partial z} + \frac{\tau_{rr} - \tau_{\phi\phi}}{r}, \tag{3.3}$$

$$\rho\left(u\frac{\partial u}{\partial r} + w\frac{\partial v}{\partial z} - \frac{uv}{r}\right) = \frac{1}{r^2}\frac{\partial}{\partial r}\left(r^2\tau_{r\phi}\right) + \frac{\partial \tau_{z\phi}}{\partial z} + \frac{\tau_{r\phi} - \tau_{\phi r}}{r}, \tag{3.4}$$

$$\rho\left(u\frac{\partial w}{\partial r} + w\frac{\partial w}{\partial z}\right) = \frac{1}{r}\frac{\partial}{\partial r}\left(r\tau_{rz}\right) + \frac{\partial \tau_{zz}}{\partial z}, \tag{3.5}$$

$$u\frac{\partial T}{\partial r} + w\frac{\partial T}{\partial z} = \alpha_m\left(\frac{1}{r}\frac{\partial T}{\partial r} + \frac{\partial^2 T}{\partial z^2} + \frac{\partial^2 T}{\partial r^2}\right)$$

$$+\frac{(\rho c)_\rho}{(\rho c)_f}\left(D_B\left(\frac{\partial T}{\partial r}\frac{\partial C}{\partial r} + \frac{\partial T}{\partial z}\frac{\partial C}{\partial z}\right)\right) + \frac{D_T}{T_\infty}\left(\left(\frac{\partial T}{\partial r}\right)^2 + \left(\frac{\partial T}{\partial r}\right)^2\right), \tag{3.6}$$

$$u\frac{\partial C}{\partial r} + w\frac{\partial C}{\partial z} = D_B\left(\frac{1}{r}\frac{\partial C}{\partial r} + \frac{\partial^2 C}{\partial z^2} + \frac{\partial^2 C}{\partial r^2}\right) + \frac{D_T}{T_\infty}\left(\frac{1}{r}\frac{\partial T}{\partial r} + \frac{\partial^2 T}{\partial z^2} + \frac{\partial^2 T}{\partial r^2}\right). \tag{3.7}$$

As we know from defination of tensor

$$\tau_{ij} = -pI + \mu e + \mu_c e^2. \tag{3.8}$$

τ_{ij} in matrix form

$$\tau_{ij} = \begin{bmatrix} \tau_{rr} & \tau_{r\phi} & \tau_{rz} \\ \tau_{\phi r} & \tau_{\phi\phi} & \tau_{\phi z} \\ \tau_{zr} & \tau_{z\phi} & \tau_{zz} \end{bmatrix}, \tag{3.9}$$

and deformation rate tensor e in matrix form

$$\begin{aligned}
e = \nabla V + (\nabla V)^T &= \begin{bmatrix} \frac{\partial u}{\partial r} & \frac{1}{r}\frac{\partial u}{\partial \phi} - \frac{v}{r} & \frac{\partial u}{\partial z} \\ \frac{\partial v}{\partial r} & \frac{1}{r}\frac{\partial v}{\partial \phi} + \frac{u}{r} & \frac{\partial v}{\partial z} \\ \frac{\partial w}{\partial r} & \frac{1}{r}\frac{\partial w}{\partial \phi} & \frac{\partial w}{\partial z} \end{bmatrix} + \begin{bmatrix} \frac{\partial u}{\partial r} & \frac{\partial v}{\partial r} & \frac{\partial w}{\partial r} \\ \frac{1}{r}\frac{\partial u}{\partial \phi} - \frac{v}{r} & \frac{1}{r}\frac{\partial v}{\partial \phi} + \frac{u}{r} & \frac{1}{r}\frac{\partial w}{\partial \phi} \\ \frac{\partial u}{\partial z} & \frac{\partial v}{\partial z} & \frac{\partial w}{\partial z} \end{bmatrix} \\
&= \begin{bmatrix} 2\frac{\partial u}{\partial r} & \frac{1}{r}\frac{\partial u}{\partial \phi} + \frac{\partial v}{\partial r} - \frac{v}{r} & \frac{\partial u}{\partial z} + \frac{\partial w}{\partial r} \\ \frac{\partial v}{\partial r} + \frac{1}{r}\frac{\partial u}{\partial \phi} - \frac{v}{r} & 2\frac{1}{r}\frac{\partial v}{\partial \phi} + \frac{u}{r} & \frac{\partial v}{\partial z} + \frac{1}{r}\frac{\partial w}{\partial \phi} \\ \frac{\partial w}{\partial r} + \frac{\partial u}{\partial z} & \frac{1}{r}\frac{\partial w}{\partial \phi} + \frac{\partial v}{\partial z} & 2\frac{\partial w}{\partial z} \end{bmatrix}.
\end{aligned} \tag{3.10}$$

The azimuthal coordinate is independent of the velocity profile due to axial symmetry.
$\frac{\partial u}{\partial \phi} = \frac{\partial v}{\partial \phi} = \frac{\partial w}{\partial \phi} = 0.$

$$e = \begin{bmatrix} 2\frac{\partial u}{\partial r} & \frac{\partial v}{\partial r} - \frac{v}{r} & \frac{\partial u}{\partial z} + \frac{\partial w}{\partial r} \\ \frac{\partial v}{\partial r} - \frac{v}{r} & 2\frac{u}{r} & \frac{\partial v}{\partial z} \\ \frac{\partial w}{\partial r} + \frac{\partial u}{\partial z} & \frac{\partial v}{\partial z} & 2\frac{\partial w}{\partial z} \end{bmatrix}, \tag{3.11}$$

The product of deformation tensor is as under:

$$e^2 = e.e = \begin{bmatrix} 2\frac{\partial u}{\partial r} & \frac{\partial v}{\partial r} - \frac{v}{r} & \frac{\partial u}{\partial z} + \frac{\partial w}{\partial r} \\ \frac{\partial v}{\partial r} - \frac{v}{r} & 2\frac{u}{r} & \frac{\partial v}{\partial z} \\ \frac{\partial w}{\partial r} + \frac{\partial u}{\partial z} & \frac{\partial v}{\partial z} & 2\frac{\partial w}{\partial z} \end{bmatrix} . \begin{bmatrix} 2\frac{\partial u}{\partial r} & \frac{\partial v}{\partial r} - \frac{v}{r} & \frac{\partial u}{\partial z} + \frac{\partial w}{\partial r} \\ \frac{\partial v}{\partial r} - \frac{v}{r} & 2\frac{u}{r} & \frac{\partial v}{\partial z} \\ \frac{\partial w}{\partial r} + \frac{\partial u}{\partial z} & \frac{\partial v}{\partial z} & 2\frac{\partial w}{\partial z} \end{bmatrix},$$

$$e^2 = \begin{bmatrix} 4\left(\frac{\partial u}{\partial r}\right)^2 & 2\frac{\partial u}{\partial r}\left(\frac{\partial v}{\partial r} - \frac{v}{r}\right) & 2\frac{\partial u}{\partial r}\left(\frac{\partial u}{\partial z} + \frac{\partial w}{\partial r}\right) \\ +\left(\frac{\partial v}{\partial r} - \frac{v}{r}\right)^2 & +\left(\frac{\partial v}{\partial r} - \frac{v}{r}\right)^2 & +\frac{\partial v}{\partial z}\left(\frac{\partial v}{\partial r} - \frac{v}{r}\right) \\ +\left(\frac{\partial u}{\partial z} + \frac{\partial w}{\partial r}\right)^2 & +\frac{\partial v}{\partial z}\left(\frac{\partial u}{\partial z} + \frac{\partial w}{\partial r}\right) & +2\frac{\partial w}{\partial z}\left(\frac{\partial u}{\partial z} + \frac{\partial w}{\partial r}\right) \\ 2\frac{\partial u}{\partial r}\left(\frac{\partial v}{\partial r} - \frac{v}{r}\right) & \left(\frac{\partial v}{\partial r} - \frac{v}{r}\right)^2 & \left(\frac{\partial v}{\partial r} - \frac{v}{r}\right)\left(\frac{\partial u}{\partial z} + \frac{\partial w}{\partial r}\right) \\ +2\frac{u}{r}\left(\frac{\partial v}{\partial r} - \frac{v}{r}\right) & +4\left(\frac{u}{r}\right)^2 & +2\frac{u}{r}\frac{\partial v}{\partial z} \\ +\frac{\partial v}{\partial z}\left(\frac{\partial w}{\partial r} + \frac{\partial u}{\partial z}\right) & +\left(\frac{\partial v}{\partial z}\right)^2 & +2\frac{\partial v}{\partial z}\frac{\partial w}{\partial z} \\ 2\frac{\partial u}{\partial r}\left(\frac{\partial w}{\partial r} + \frac{\partial u}{\partial z}\right) & \left(\frac{\partial w}{\partial r} + \frac{\partial u}{\partial z}\right)\left(\frac{\partial v}{\partial r} - \frac{v}{r}\right) & \left(\frac{\partial w}{\partial r} + \frac{\partial u}{\partial z}\right)^2 \\ +\frac{\partial v}{\partial z}\left(\frac{\partial v}{\partial r} - \frac{v}{r}\right) & +2\frac{u}{r}\frac{\partial v}{\partial z} & +\left(\frac{\partial v}{\partial z}\right)^2 \\ +2\frac{\partial w}{\partial z}\left(\frac{\partial w}{\partial r} + \frac{\partial u}{\partial z}\right) & +2\frac{\partial v}{\partial z}\frac{\partial w}{\partial z} & +4\left(\frac{\partial w}{\partial z}\right)^2 \end{bmatrix}. \tag{3.12}$$

By putting values in Eq. (3.8), we get

$$\begin{bmatrix} \tau_{rr} & \tau_{r\phi} & \tau_{rz} \\ \tau_{\phi r} & \tau_{\phi\phi} & \tau_{\phi z} \\ \tau_{zr} & \tau_{z\phi} & \tau_{zz} \end{bmatrix} = -p \begin{bmatrix} 1 & 0 & 0 \\ 0 & 1 & 0 \\ 0 & 0 & 1 \end{bmatrix} + \mu \begin{bmatrix} 2\frac{\partial u}{\partial r} & \frac{\partial v}{\partial r} - \frac{v}{r} & \frac{\partial u}{\partial z} + \frac{\partial w}{\partial r} \\ \frac{\partial v}{\partial r} - \frac{v}{r} & 2\frac{u}{r} & \frac{\partial v}{\partial z} \\ \frac{\partial w}{\partial r} + \frac{\partial u}{\partial z} & \frac{\partial v}{\partial z} & 2\frac{\partial w}{\partial z} \end{bmatrix}$$

$$
+\mu_c
\begin{bmatrix}
\begin{array}{c}
4\left(\frac{\partial u}{\partial r}\right)^2 \\
+\left(\frac{\partial v}{\partial r}-\frac{v}{r}\right)^2 \\
+\left(\frac{\partial u}{\partial z}+\frac{\partial w}{\partial r}\right)^2
\end{array}
&
\begin{array}{c}
2\frac{\partial u}{\partial r}\left(\frac{\partial v}{\partial r}-\frac{v}{r}\right) \\
+\left(\frac{\partial v}{\partial r}-\frac{v}{r}\right)^2 \\
+\frac{\partial v}{\partial z}\left(\frac{\partial u}{\partial z}+\frac{\partial w}{\partial r}\right)
\end{array}
&
\begin{array}{c}
2\frac{\partial u}{\partial r}\left(\frac{\partial u}{\partial z}+\frac{\partial w}{\partial r}\right) \\
+\frac{\partial v}{\partial z}\left(\frac{\partial v}{\partial r}-\frac{v}{r}\right) \\
+2\frac{\partial w}{\partial z}\left(\frac{\partial u}{\partial z}+\frac{\partial w}{\partial r}\right)
\end{array}
\\[2em]
\begin{array}{c}
2\frac{\partial u}{\partial r}\left(\frac{\partial v}{\partial r}-\frac{v}{r}\right) \\
+2\frac{u}{r}\left(\frac{\partial v}{\partial r}-\frac{v}{r}\right) \\
+\frac{\partial v}{\partial z}\left(\frac{\partial w}{\partial r}+\frac{\partial u}{\partial z}\right)
\end{array}
&
\begin{array}{c}
\left(\frac{\partial v}{\partial r}-\frac{v}{r}\right)^2 \\
+\left(2\frac{u}{r}\right)^2+\left(\frac{\partial v}{\partial z}\right)^2
\end{array}
&
\begin{array}{c}
\left(\frac{\partial v}{\partial r}-\frac{v}{r}\right)\left(\frac{\partial u}{\partial z}+\frac{\partial w}{\partial r}\right) \\
+2\frac{u}{r}\frac{\partial v}{\partial z}+2\frac{\partial v}{\partial z}\frac{\partial w}{\partial z}
\end{array}
\\[2em]
\begin{array}{c}
2\frac{\partial u}{\partial r}\left(\frac{\partial w}{\partial r}+\frac{\partial u}{\partial z}\right) \\
+\frac{\partial v}{\partial z}\left(\frac{\partial v}{\partial r}-\frac{v}{r}\right) \\
+2\frac{\partial w}{\partial z}\left(\frac{\partial w}{\partial r}+\frac{\partial u}{\partial z}\right)
\end{array}
&
\begin{array}{c}
\left(\frac{\partial w}{\partial r}+\frac{\partial u}{\partial z}\right)\left(\frac{\partial v}{\partial r}-\frac{v}{r}\right) \\
+2\frac{u}{r}\frac{\partial v}{\partial z}+2\frac{\partial v}{\partial z}\frac{\partial w}{\partial z}
\end{array}
&
\begin{array}{c}
\left(\frac{\partial w}{\partial r}+\frac{\partial u}{\partial z}\right)^2 \\
+\left(\frac{\partial v}{\partial z}\right)^2+\left(2\frac{\partial w}{\partial z}\right)^2
\end{array}
\end{bmatrix}
. \tag{3.13}
$$

The stress tensor, pressure, cross-viscosity coefficient, Kronecker symbol, and deformation rate tensor are denoted as τ_{ij}, p, μ_{ij}, δ_{ij}, and e_{ij}, respectively. The deformation rate tensor's constituents are $e_{rr}=2\frac{\partial u}{\partial r}$, $e_{\phi\phi}=2\frac{u}{r}$, $e_{zz}=2\frac{\partial w}{\partial z}$, $e_{r\phi}=e_{\phi r}=r\frac{\partial}{\partial r}\left(\frac{v}{r}\right)$, $e_{z\phi}=e_{\phi z}=\frac{\partial v}{\partial z}$, $e_{rz}=e_{zr}=\frac{\partial u}{\partial z}+\frac{\partial w}{\partial r}$. The stress tensor components are defined from Eq. (3.13) as follows:

$$
\tau_{rr}=-p+\mu\left(2\frac{\partial u}{\partial r}\right)+\mu_c\left\{4\left(\frac{\partial u}{\partial r}\right)^2+\left(\frac{\partial u}{\partial z}+\frac{\partial w}{\partial r}\right)^2+\left(\frac{\partial v}{\partial r}-\frac{v}{r}\right)^2\right\}, \tag{3.14}
$$

$$
\tau_{zr}=\mu\left(\frac{\partial u}{\partial z}+\frac{\partial w}{\partial r}\right)+\mu_c\left\{\begin{array}{c}\left(\frac{\partial u}{\partial z}+\frac{\partial w}{\partial r}\right)\left(2\frac{\partial u}{\partial r}\right)+\left(\frac{\partial v}{\partial z}\right)\left(\frac{\partial v}{\partial r}-\frac{v}{r}\right) \\ +\left(2\frac{\partial w}{\partial z}\right)\left(\frac{\partial u}{\partial z}+\frac{\partial w}{\partial r}\right)\end{array}\right\}, \tag{3.15}
$$

$$
\tau_{\phi\phi}=-p+\mu\left(2\frac{u}{r}\right)+\mu_c\left\{4\frac{u^2}{r^2}+\left(\frac{\partial v}{\partial z}\right)^2+\left(\frac{\partial v}{\partial r}-\frac{v}{r}\right)^2\right\}, \tag{3.16}
$$

$$
\tau_{r\phi}=\mu\left(\frac{\partial v}{\partial r}-\frac{v}{r}\right)+\mu_c\left\{\begin{array}{c}\left(\frac{\partial v}{\partial r}-\frac{v}{r}\right)\left(2\frac{\partial u}{\partial r}\right)+\left(\frac{2u}{r}\right)\left(\frac{\partial v}{\partial r}-\frac{v}{r}\right) \\ +\left(\frac{\partial v}{\partial z}\right)\left(\frac{\partial u}{\partial z}+\frac{\partial w}{\partial r}\right)\end{array}\right\}, \tag{3.17}
$$

$$
\tau_{z\phi}=\mu\frac{\partial v}{\partial z}+\mu_c\left\{\left(\frac{\partial u}{\partial z}+\frac{\partial w}{\partial r}\right)\left(\frac{\partial v}{\partial r}-\frac{v}{r}\right)+2\left(\frac{\partial v}{\partial z}\right)\left(\frac{u}{r}\right)+\left(\frac{\partial w}{\partial z}\right)\left(\frac{\partial v}{\partial z}\right)\right\}, \tag{3.18}
$$

$$
\tau_{zz}=-p+2\mu\left(\frac{\partial w}{\partial z}\right)+\mu_c\left\{\left(2\frac{\partial w}{\partial z}\right)^2+\left(\frac{\partial v}{\partial z}\right)^2+\left(\frac{\partial u}{\partial z}+\frac{\partial w}{\partial r}\right)^2\right\}. \tag{3.19}
$$

The physical boundaries are as follows:

$$u = \beta_1 \tau_{rz}, \ v = \beta_2 \tau_{z\phi} + r\omega, \ w = 0, \ T = T_w + \beta_3 T_z,$$

$$C = C_w + \beta_4 C_z \ \text{at} \ z = 0,$$

$$u \rightarrow 0, \ v \rightarrow 0, \ T \rightarrow T_\infty, \ C \rightarrow C_\infty \ \text{as} \ z \rightarrow \infty, \tag{3.20}$$

where thermal diffusivity is $\alpha_m = \frac{k}{(\rho c)_f}$, capacity of nanoparticles k, thermal conductivity $(\rho c)_p$ and heat capacity of the base fluid $(\rho c)_f$. T and C stand for fluid temperature and concentration, ρ is fluid density, T_w is temperature and C_w is concentration of nanoparticles at the moving boundary surface, The temperature and concentration of nanoparticles distant from the sheet are T_∞ and C_∞ and the Brownian diffusion coefficient is D_B, Thermophoresis diffusion coefficient is D_T, with radial slip as β_1, azimuthal slip as β_2, thermal slip as β_3, and concentration slip as β_4 coefficients. By introducing similarity transformation,

$$\zeta = z\sqrt{\frac{\omega}{\nu}}, \ u = r\omega f'(\zeta), \ v = r\omega g(\zeta), \ w = -2\sqrt{\nu\omega}f(\zeta),$$

$$p = p_\infty - \mu\omega P(\zeta), \ T = T_\infty + (T_w - T_\infty)\theta(\zeta), \ C = C_\infty + (C_w - C_\infty)\phi(\zeta). \tag{3.21}$$

The similarity variable is ζ, the stream functions are f, g the temperature is θ and the concentration function is ϕ are non-dimensional. We may construct the following ordinary differential equations by using above equations:

$$f''' - f'^2 + 2ff'' + g^2 + K(f''^2 - 2f'f''' - g'^2) = 0, \tag{3.22}$$

$$g'' - 2f'g + 2fg' - 2K(f'g'' - f''g') = 0, \tag{3.23}$$

$$\theta'' + P_r(f\theta' + N_b\theta'\phi' + N_t\theta'^2) = 0, \tag{3.24}$$

$$\phi'' + \frac{N_t}{N_b}\theta'' + S_c f\phi' = 0, \tag{3.25}$$

24

where $K = \frac{\mu_c \omega}{\mu}$ and $P_r = \frac{\mu C_p}{k}$ material parameters of Riener Rivlin fluid and the Prandtl number. The thermophoresis parameter is $N_t = \frac{\tau D_T (T_f - T_\infty)}{k T_\infty}$, the Brownian motion parameter is $N_b = \frac{\tau D_B (C_w - C_\infty)}{k}$, the differentiation with regard to ζ is denoted by the prime. The associated boundary conditions are as follows:

$$
\begin{aligned}
f(0) &= 0, \ f'(0) = \alpha_1 f''(0) \left[1 - 2K f'(0)\right], \ g(0) = \alpha_2 g'(0) \left[1 - 2K f'(0)\right], \\
\theta(0) &= 1 + \beta \theta'(0), \ \phi(0) = 1 + \gamma \phi'(0) \quad \text{at} \quad \zeta = 0, \\
f' &\rightarrow 0, \ g \rightarrow 0, \ \phi \rightarrow 0 \quad \text{as} \quad \zeta \rightarrow \infty.
\end{aligned}
\tag{3.26}
$$

The radial, azimuthal, thermal, and concentration slip coefficients are α_1, α_2, β and γ respectively. The presence of viscosity at the surface causes tangential tension, which causes resistance in disk rotation. The torque T_0 is calculated using a definite integral, such as

$$
T_0 = - \int_0^R \tau_{z\phi}\big|_{z=0} \left(2\pi r^2\right) dr = - \frac{\pi \rho \omega}{2} \sqrt{\omega \upsilon} R^4 G'(0).
\tag{3.27}
$$

Skin friction coefficient C_f, local Nusselt number N_u, and Sherwood number S_h are the physical quantities of importance, and they are defined as:

$$
C_f = \frac{\sqrt{\tau_r^2 - \tau_\phi^2}}{\rho (r\omega)^2}, \ N_u = \frac{r q_w}{k (T_w - T_\infty)}, \ S_h = \frac{r j_w}{D_B (C_w - C_\infty)}.
\tag{3.28}
$$

When these values are transformed, they become:

$$
\begin{aligned}
C_f &= \left(\frac{\omega r^2}{\upsilon}\right)^{-\frac{1}{2}} \sqrt{(F''(0))^2 - (G'(0))^2}, \ Nu = \left(\frac{\omega r^2}{\upsilon}\right)^{\frac{1}{2}} \theta'(0), \\
Sh &= \left(\frac{\omega r^2}{\upsilon}\right)^{-\frac{1}{2}} \phi'(0), \ \text{where} \ \mathrm{Re} = \frac{\omega r^2}{\upsilon} \ \text{is rotational Reynold number.} \quad (3.29)
\end{aligned}
$$

3.2 Numerical solution

The system of linked non-linear (ODEs) is transformed to a first order differential equation using the shooting procedure in which f is considered as y_1, g as y_4, θ as y_6 and ϕ as y_8.

$$y_1' = y_2, \tag{3.30}$$

$$y_2' = y_3, \tag{3.31}$$

$$y_3' = y_1^2 - 2y_1y_3 - y_4^2 - K\left(-y_3^2 + 2y_1' + y_5^2\right), \tag{3.32}$$

$$y_4' = y_5, \tag{3.33}$$

$$y_5' = y_2y_4 - 2y_1\ y_5 - 2K\left(y_2y_4' - y_2y_5\right), \tag{3.34}$$

$$y_6' = y_7, \tag{3.35}$$

$$y_7' = -2P_r\left(y_1y_7 + N_by_7y_8 + N_ty_8^2\right), \tag{3.36}$$

$$y_8' = y_9, \tag{3.37}$$

$$y_9' = -\frac{N_t}{N_b}y_9 - S_cy_2y_9, \tag{3.38}$$

with associated boundary conditions

$$
\begin{aligned}
y_1(0) &= 0,\ y_2(0) = \alpha_1y_3(0)\left[1 - 2Ky_1(0)\right], \\
y_4(0) &= \alpha_2y_5(0)\left[1 - 2Ky_2(0)\right], \\
y_6(0) &= 1 + \beta y_7(0),\ y_8(0) = 1 + \gamma y_9(0), \\
y_2(\infty) &\to 0,\ y_4(\infty) \to 0,\ y_6(\infty) \to 0,\ y_8(\infty) \to 0. \tag{3.39}
\end{aligned}
$$

continuous mesh selection and error control are employed for all residuals solution calculations. For this, bvp4c (a MATLAB function) used. This makes use of the three-stage Lobatto formula with finite difference.

3.3 Results and discussion

An unending spinning disk with several slip situations produces a Reiner Rivlin nanofluid. The ReinerRivlin fluid and numerous slip situations are effectively counted numerically. Table 1 shows the Reiner Rivlin fluid and various slip situations are effectively counted numerically. skin friction, radial and azimuthal wall stress and radial and azimuthal wall stress. The entrainment velocity $f(\infty)$ can be used to calculate the volumetric flow rate in the von-Karman issue. This is driving torque, which is measured as $g\prime(0)$ on the disk. When viscoelastic effects are present in the von Karman issue, The data in Table 2 can be used to forecast this phenomena. When the radial and azimuthal slip coefficient increases resistive torque and skin friction increase. This demonstrate that a longer azimuthal slip coefficient leads in increased torque at the disk shaft. Table 2 displays the findings for Nusselt and Sherwood number for various values of the Reiner-Rivlin fluid parameter, concentration and temperature slip, Brownian and thermophoretic parameters, Prandtl and Schmidt numbers. The Table show the Nusselt number for Schmidt number, thermal slip, Brownian motion, thermophoretic coefficient and Reiner-Rivlin parameter are all increasing. Physically, the rate of heat transmission increases when these parameters are increased. The heat transfer rate reverses when the concentration slip parameter and Prandtl number are used. Sherwood number is now a function of Reiner-Rivlin fluid parameter, concentration slip parameter, thermal slip parameter, thermophoretic parameter, and Prandtl number, and it is rising. Brownian motion parameter and Schmidt number, on the other hand, exhibit a declining trend.

When $K = 1$, α_1 and α_2 are identical, Figures 3.2(a-e) displays the wall slip data related to the Reiner-Rivlin parameter. The wall slip tends to minimize the produced axial motion distant from the disk, but it has no effect near the wall areas. The radial velocity profile f' asymptotically disappears after reaching its maximum value in the absence of slip, despite starting from zero outside the boundary layer. It should be notice when the velocity advance closer to the wall, the slip effect becomes stronger. Increases in wall roughness characteristics cause radial velocity to rise far from the disk while decreasing

near it. The rotating impact of the disk, which is partially transmitted in the adjoining fluid layers, causes a decrease in azimuthal velocity component. Unlike the velocity profiles, the temperature and concentration profiles appear to grow as the wall slip parameters are increased. As follows, this is clarified. As the wall slip parameters increase, the amount of (cold) liquid pushed into the crucial direction decreases, resulting in an increase in liquid temperature in the limit layer. Figures 3.3(a-e) show the Reiner-Rivlin fluid parameter curves for velocity, temperature, and concentration profiles when the wall roughness is uniform. As the Reiner-Rivlin fluid parameter increases towards the disk, the radial and axial velocity profiles diminish. When K is increased, the absolute maximum also occurs at a reduced vertical distance. Physically, increased viscoelastic effects result in more fluid being pushed away in the radial direction and less fluid being pulled axially. Physically, increased viscoelastic effects result in more fluid being pushed away in the radial direction and less fluid being pulled axially. The traditional von Kármán issue preserves centrifugal fan-like behaviour in the non-Newtonian situation, as seen above. In contrast to the radial and axial velocity profiles, the azimuthal velocity profile emerges when the value of the Reiner-Rivlin fluid parameter increases. These results are the same as the results of the material parameter's second grade fluid. The behaviour of temperature slip, thermophoretic parameter, Brownian motion parameter, and Prandtl number on a temperature profile is depicted in Figures 3.4(a-d). The temperature profile is affected by both the thermophoretic and Brownian motion parameters. When these two factors are increased, the temperature profile shows a rising trend. On the other hand, the temperature profile for slip and Prandtl number exhibits the exact opposite trend. The influence of the Schmidt number, concentration slip, Brownian motion parameter and thermophoretic parameter on the concentration profile is provided at the end. We can observe that the concentration profile decreases as the Schmidt number, concentration slip, and Brownian motion parameter increase. However, raising the thermophoretic parameter has a distinct influence on the concentration profile Figures 3.5(a-d).

Table 1: The results of calculations for different values of wall roughness and Reiner-Rivlin parameters include entrainment velocity, radial and azimuthal wall tension, and skin friction.

α_1	α_2	K	$f(\infty)$	$f''(0)$	$g'(0)$	$\sqrt{f''(0)^2 + g'(0)^2}$
1	2	1	0.28989110	0.088290021	-0.29398610	0.306957112
1.5			0.29895421	0.073879008	-0.30498100	0.313802023
2			0.30529501	0.063745107	-0.31286011	0.319288014
	3		0.27778212	0.051863104	-0.23526923	0.240918105
	4	1	0.25612601	0.043912022	-0.18831304	0.193365009
		0.2	0.37288623	0.128140013	-0.40540807	0.425177112
		0.7	0.31729011	0.064287412	-0.30253509	0.309290106

Table 2: Results of $-\theta'(0)$ and $-\phi'(0)$ computations for various values of K, γ, β, N_b, N_t, Pr and Sc.

K	γ	β	N_b	N_t	Pr	Sc	$-\theta'(0)$	$-\phi'(0)$
0.2	1		0.6	0.1	5	4	0.157673	0.349707
1							0.145262	0.334920
	0.7						0.133246	0.382728
	0.8						0.139229	0.368076
		0.5	0.3	0.3	7	1	0.263466	0.090660
			0.4	0.2	5	3	0.185088	0.329659
			0.5				0.157831	0.338375
			0.6				0.133116	0.343528
				0.1		4	0.158639	0.304242
				0.3	4	1	0.227942	0.104459
					6		0.240158	0.096216
				0.1	5	3	0.158639	0.304242
						4	0.150336	0.341847
						5	0.145726	0.371408

29
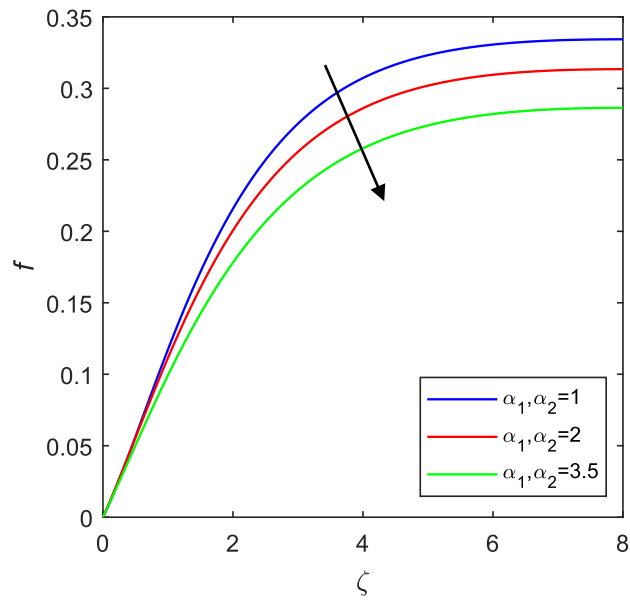
Figure 3.2(a) Plot of f for wall roughness parameters.
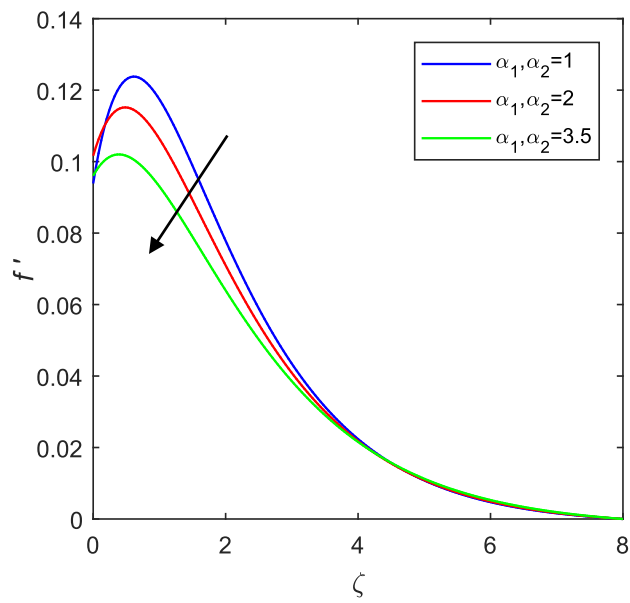
Figure 3.2(b) Plot f' for wall roughness parameters.
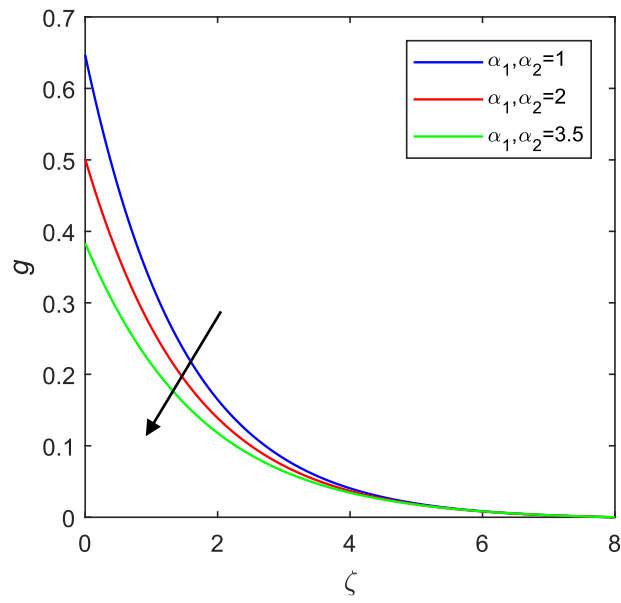
Figure 3.2(c) Plot of g for wall roughness parameters.
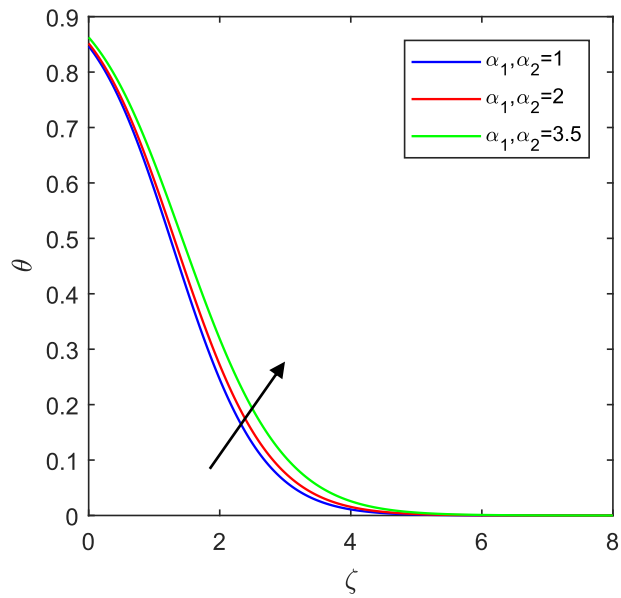
Figure 3.2(d) Plot of temperature for wall roughness parameters.
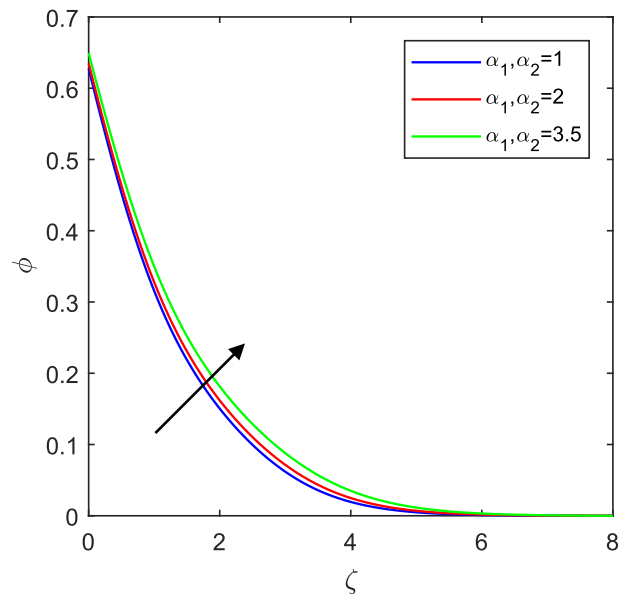
Figure 3.2(e) Plot of concentration for wall roughness parameters.
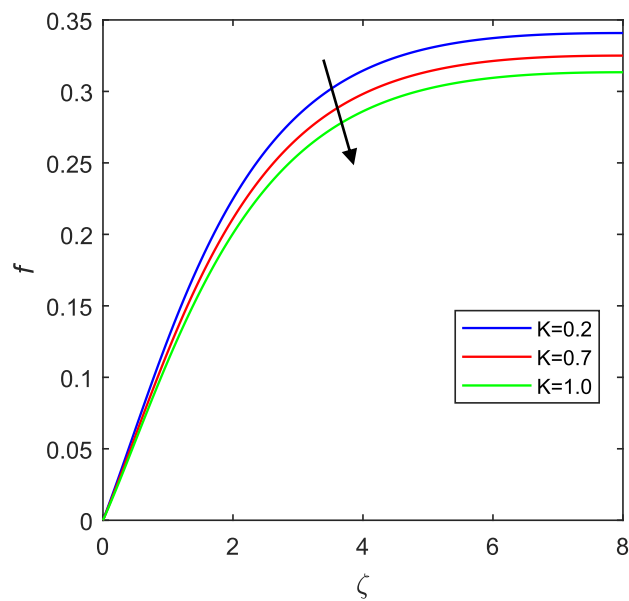
Figure 3.3(a) Plot of f for fluid parameter.
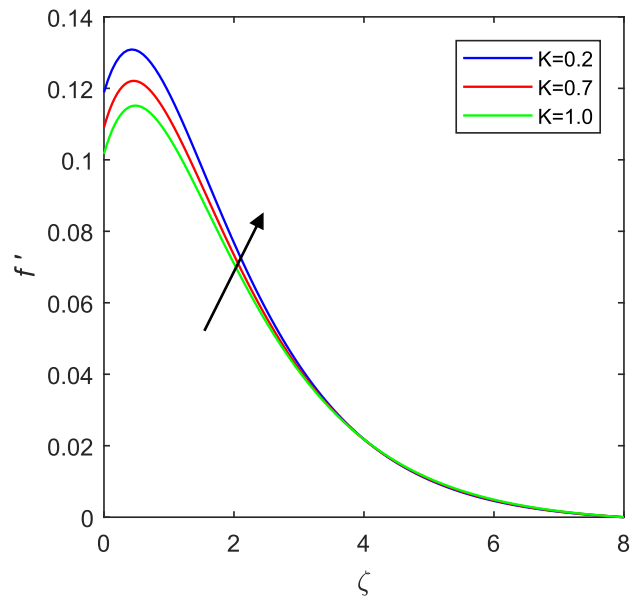
Figure 3.3(b) Plot of f' for fluid parameter.
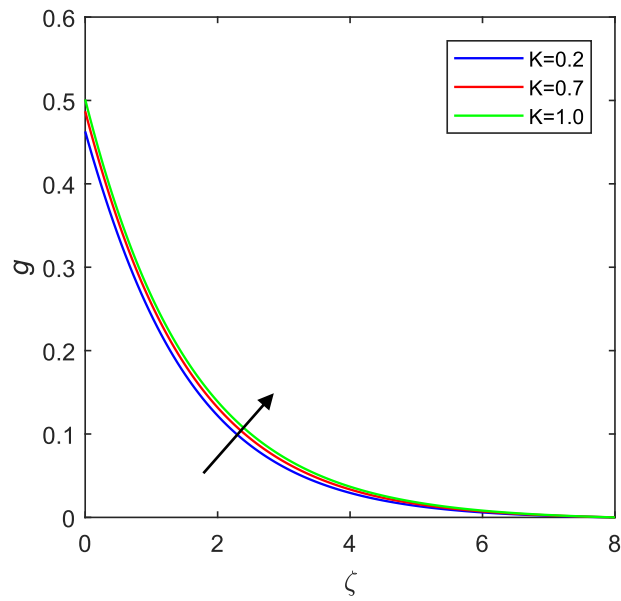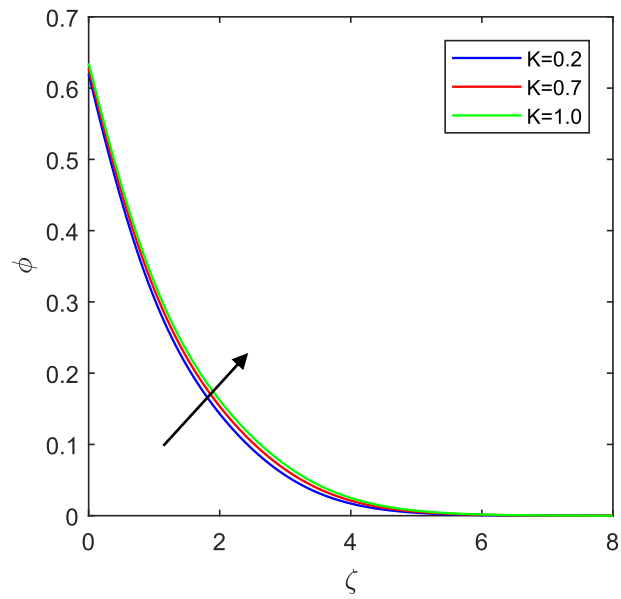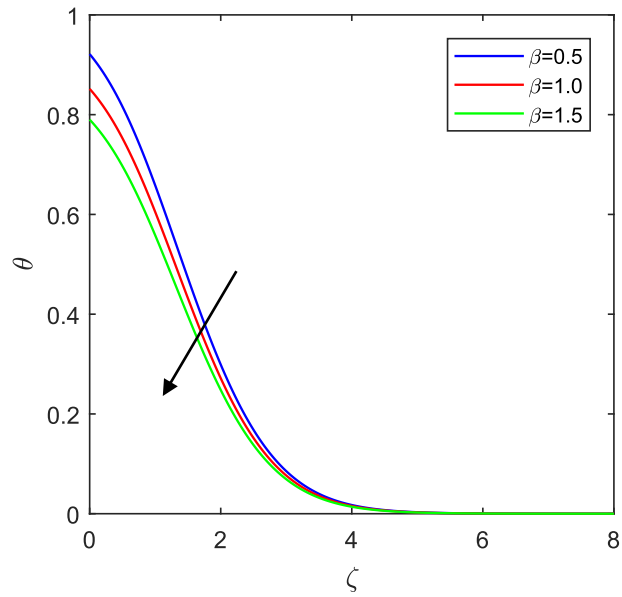

Figure 3.3(c) Plot of g for fluid parameter.
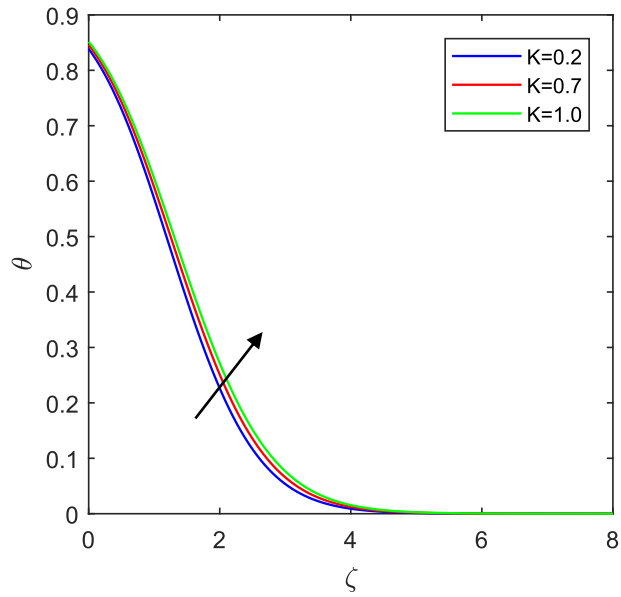
Figure 3.3(d) Plot of temperature for fluid parameter.

Figure 3.3(e) Plot of concentration for fluid parameter.

Figure 3.4(a) Plot of temperature slip for temperature profile.
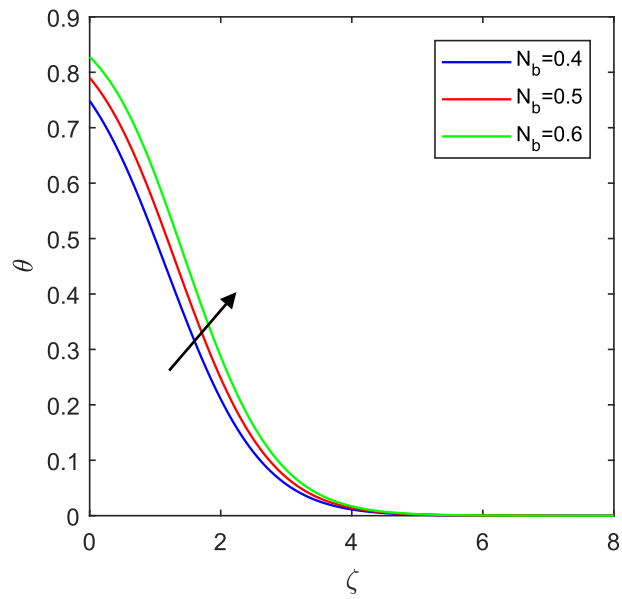
Figure 3.4(b) Plot of Brownian motion parameter for temperature profile.
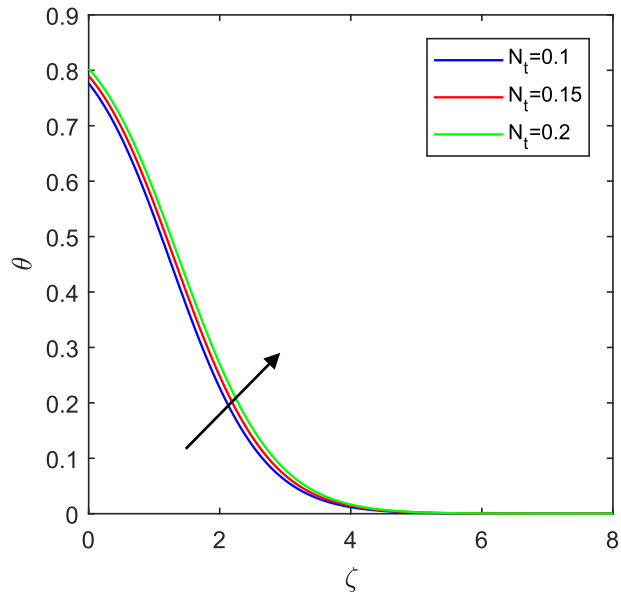
Figure 3.4(c) Plot of thermophoretic parameter for temperature profile.
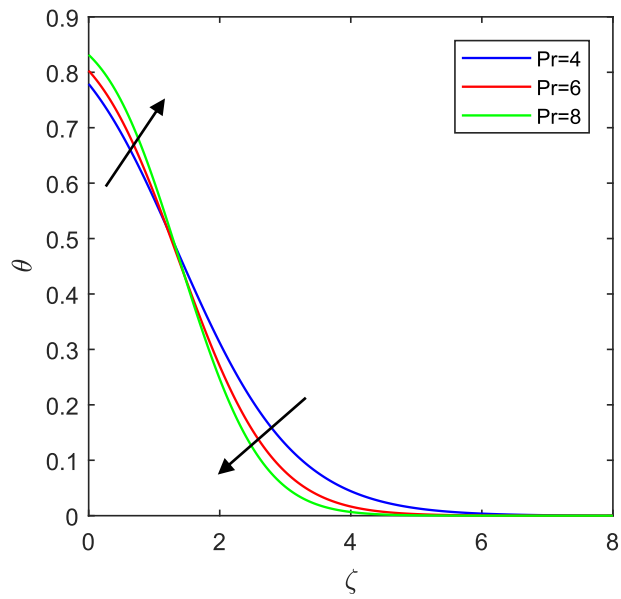
Figure 3.4(d) Plot of Prandtl number for temperature profile.
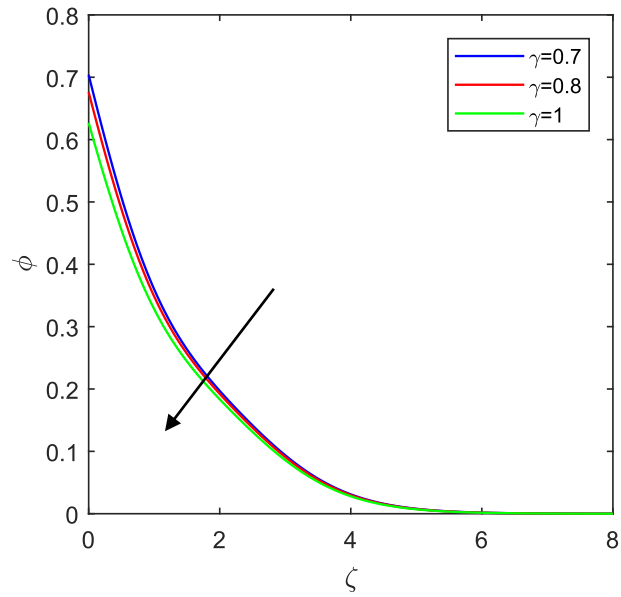
Figure 3.5(a) Plot of concentration slip for concentration profile.
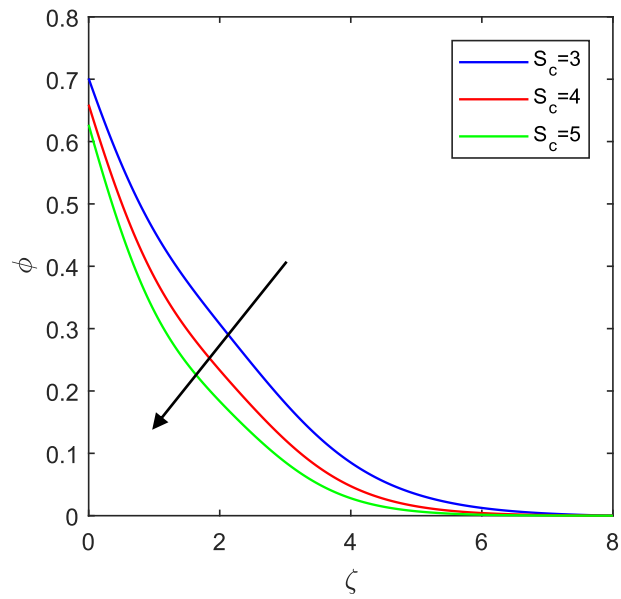
Figure 3.5(b) Plot of Schmidt number for concentration profile.
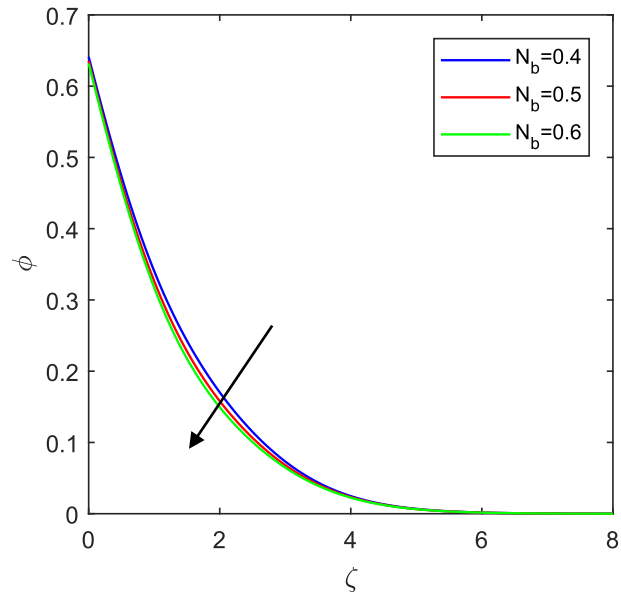
Figure 3.5(c) Plot of Brownian motion parameter for concentration profile.
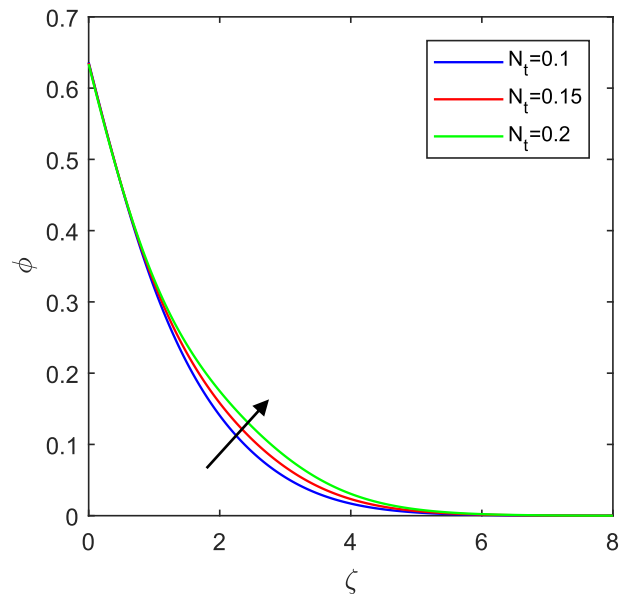
Figure 3.5(d) Plot of thermophoretic parameter for concentration profile.

Chapter 4

Impact of Cattaneo-Christov double diffusion on a Sutterby nanofluid flow over a rotating disk with Hall current and Ion slip

In this study we analyze the steady, incompressible flow of Sutterby nanofluid over a spinning disk with Hall and Ion slip effects. The disk is rotating around the vertical axis at a fixed angular velocity, generating a swirl in the fluid layers around it. The Cattaneo-Christov (CC) model is used to improve the accuracy of the traditional models for heat and mass flux, such as the Fourier and Fick models. In the fluid flow, motile micororganisms are also incorporated. The boundary layer thickness is greater than the typical scale, thus concentration slip, temperature, and velocity conditions are used. The current investigation used the temperature fluctuation condition. The appropriate similarity variables are used to transform partial differential equations to Ordinary differential equations.

4.1 Mathematical Formulation

We investigate Sutterby nanofluid flow using a stretchable rotating disk with angular velocity ω and stretching rate b. The component of velocity in the direction of r, ϕ and z are u, v and w respectively. Because of axial symmetry, the azimuthal coordinate is independent of the velocity profile. The wall temperature of the disk is T_w and the ambient temperature is T_∞, and fluid conducts through megnatic field strength (see Figure 4.1).
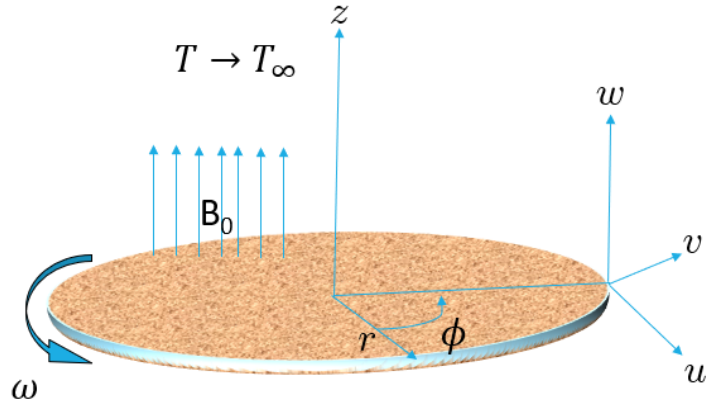
Figure 4.1 Fluid flow geometry

The stress tensor of Sutterby fluid is defined as:

$$\tau = -pI + \acute{S}, \tag{4.1}$$

$$\acute{S} = \frac{\mu_0}{2} \left[\frac{\sinh^{-1}(b\Phi)}{b\Phi} \right]^{\check{n}} . A_1, \tag{4.2}$$

with,

$$\Phi = \sqrt{\frac{Trace\,(A_1)^2}{2}}, \tag{4.3}$$

Using binomial series expension, the above equation becomes:

$$\mu \cong \frac{\mu_0}{2}\left[1 - \check{n}\frac{(b\Phi)^2}{6} + \ldots\ldots\right].$$ (4.4)

For r and z coordinates,

$$\nabla V = \begin{bmatrix} \frac{\partial u}{\partial r} & -\frac{v}{r} & \frac{\partial u}{\partial z} \\ \frac{\partial v}{\partial r} & \frac{u}{r} & \frac{\partial v}{\partial z} \\ \frac{\partial w}{\partial r} & 0 & \frac{\partial w}{\partial z} \end{bmatrix}, [\nabla V]^t = \begin{bmatrix} \frac{\partial u}{\partial r} & \frac{\partial v}{\partial r} & \frac{\partial w}{\partial r} \\ -\frac{v}{r} & \frac{u}{r} & 0 \\ \frac{\partial u}{\partial z} & \frac{\partial v}{\partial z} & \frac{\partial w}{\partial z} \end{bmatrix},$$ (4.5)

$$A_1 = \nabla V + (\nabla V)^t = \begin{bmatrix} 2\frac{\partial u}{\partial r} & \frac{\partial v}{\partial r} - \frac{v}{r} & \frac{\partial w}{\partial r} + \frac{\partial u}{\partial z} \\ \frac{\partial v}{\partial r} - \frac{v}{r} & 2\frac{u}{r} & \frac{\partial v}{\partial z} \\ \frac{\partial u}{\partial z} + \frac{\partial w}{\partial r} & \frac{\partial v}{\partial z} & 2\frac{\partial w}{\partial z} \end{bmatrix},$$ (4.6)

$$\Phi^2 = \left(\frac{\partial w}{\partial r} + \frac{\partial u}{\partial z}\right)^2 + 2\left[\left(\frac{\partial u}{\partial r}\right)^2 + \left(\frac{u}{r}\right)^2 + \left(\frac{\partial w}{\partial z}\right)^2\right].$$ (4.7)

The Sutterby fluid model is a dual-nature model that takes into consideration both pseudoplastic and dilatant material properties. The governing equations are as follows:

$$\frac{\partial u}{\partial r} + \frac{u}{r} + \frac{\partial w}{\partial z} = 0,$$ (4.8)

$$\rho\left(u\frac{\partial u}{\partial r} + w\frac{\partial u}{\partial z} - \frac{v^2}{r}\right) = \frac{2}{r}\frac{\partial}{\partial z}\left(r^2\mu\frac{\partial u}{\partial r}\right) - 2\frac{\mu u}{r^2}$$
$$+ \frac{\partial}{\partial z}\left(\mu\left(\frac{\partial u}{\partial z} + \frac{\partial w}{\partial r}\right)\right) - \frac{\sigma B_o^2}{\alpha^2 + \beta_e^2}\left(\alpha u - \beta_e v\right),$$ (4.9)

$$\rho\left(u\frac{\partial v}{\partial r} + w\frac{\partial v}{\partial z} - \frac{uv}{r}\right) = \frac{1}{r^2}\left(r^2\mu\left(\frac{\partial v}{\partial r} - \frac{v}{r}\right)\right)$$
$$+ \frac{\partial}{\partial z}\left(\mu\frac{\partial v}{\partial z}\right) - \frac{\sigma B_o^2}{\alpha^2 + \beta_e^2}\left(\alpha v + \beta_e u\right),$$ (4.10)

$$\rho\left(u\frac{\partial w}{\partial r} + w\frac{\partial v}{\partial z}\right) = \frac{1}{r}\frac{\partial}{\partial r}\left(ru\left(\frac{\partial u}{\partial z} + \frac{\partial w}{\partial r}\right)\right) + 2\frac{\partial}{\partial z}\left(\mu\frac{\partial w}{\partial z}\right),$$ (4.11)

$$u\frac{\partial T}{\partial r} + w\frac{\partial T}{\partial z} = \alpha_m\left(\frac{1}{r}\frac{\partial T}{\partial r} + \frac{\partial^2 T}{\partial z^2} + \frac{\partial^2 T}{\partial r^2}\right) + \frac{(\rho c)_\rho}{(\rho c)_f}\left(D_B\left(\frac{\partial T}{\partial r}\frac{\partial C}{\partial r} + \frac{\partial T}{\partial z}\frac{\partial C}{\partial z}\right)\right)$$
$$+ \frac{D_T}{T_\infty}\left(\left(\frac{\partial T}{\partial r}\right)^2 + \left(\frac{\partial T}{\partial r}\right)^2\right) - \lambda_e\left(\begin{array}{c} u^2\frac{\partial^2 T}{\partial r^2} + w^2\frac{\partial^2 T}{\partial z^2} + 2uw\frac{\partial^2 T}{\partial r\partial z} \\ + \left(u\frac{\partial u}{\partial r} + w\frac{\partial u}{\partial z}\right)\frac{\partial T}{\partial r} + \left(u\frac{\partial w}{\partial r} + w\frac{\partial w}{\partial z}\right)\frac{\partial T}{\partial z} \end{array}\right),$$ (4.12)

$$u\frac{\partial C}{\partial r} + w\frac{\partial C}{\partial z} = D_B\left(\frac{1}{r}\frac{\partial C}{\partial r} + \frac{\partial^2 C}{\partial z^2} + \frac{\partial^2 C}{\partial r^2}\right) + \frac{D_T}{T_\infty}\left(\frac{1}{r}\frac{\partial T}{\partial r} + \frac{\partial^2 T}{\partial z^2} + \frac{\partial^2 T}{\partial r^2}\right)$$
$$-\lambda_c\left(u\frac{\partial C}{\partial r}\frac{\partial u}{\partial r} + w\frac{\partial C}{\partial r}\frac{\partial u}{\partial z} + u\frac{\partial C}{\partial z}\frac{\partial w}{\partial r} + w\frac{\partial C}{\partial z}\frac{\partial w}{\partial z} + 2uw\frac{\partial^2 C}{\partial r\partial z} + w^2\frac{\partial^2 C}{\partial z^2} + u^2\frac{\partial^2 C}{\partial r^2}\right), \tag{4.13}$$

$$u\frac{\partial N}{\partial r} + w\frac{\partial N}{\partial z} + \frac{bw_c}{C_w - C_\infty}\left(\frac{\partial N}{\partial z}\frac{\partial C}{\partial z} + N\frac{\partial C}{\partial z}\right) = Dn\left(\frac{\partial^2 N}{\partial r^2} + \frac{1}{r}\frac{\partial N}{\partial r} + \frac{\partial^2 N}{\partial z^2}\right), \tag{4.14}$$

with associated boundary conditions:

$$u = b\omega,\ v = \omega r,\ w = 0,\ N = N_w \quad \text{at} \quad \eta = 0$$
$$u \to 0,\ v \to 0,\ N \to N_\infty \quad \text{as} \quad \eta \to \infty. \tag{4.15}$$

4.1.1   Similarity Transformation

Applying the following transformation will change PDEs into ODEs.

$$\eta = z\sqrt{\frac{\omega}{\nu}},\ u = r\omega f',\ v = r\omega g,\ w = -2\sqrt{\nu\omega}f',\ p = p_\infty - \mu\omega p,$$
$$T = T_\infty + (T_w - T_\infty)\theta,\ C = C_\infty + (C_w - C_\infty)\phi,$$
$$N = N_\infty + (N_w - N_\infty)\xi. \tag{4.16}$$

The equation of continuity is identically fulfilled using similarity transformations, and the usual non-dimensional system of equations with boundary conditions have the following form:

$$f''' - 2N\epsilon_1^2\left(f'^2 f''' + 2f' f''^2\right) = f'^2 - 2ff'' - g^2 + \frac{M}{\alpha^2 + \beta_e^2}(\alpha f' - \beta_e g), \tag{4.17}$$

$$g'' - 2N\epsilon_1^2\left(f'^2 g'' + 2f' f'' g'\right) = f'^2 + 2f'g - 2fg' + \frac{M}{\alpha^2 + \beta_e^2}(\alpha g + \beta_e f'), \tag{4.18}$$

$$\left(1 + 4\lambda_c S_c f^2\right)\phi'' = -2S_c f\phi' - \frac{N_t}{N_b}\theta'' - 4\lambda_c S_c ff'\phi', \tag{4.19}$$

$$\theta''(1 - 4\lambda_e P_r f^2) = P_r(-2f\theta' - N_b\theta'\phi' - N_t\theta'^2 + 4\lambda_e ff'\theta'), \tag{4.20}$$

$$\xi'' = -2S_b f\xi' + P_e\left\{\phi'\xi' + \left(\frac{1}{\sigma_3} + \xi\right)\phi''\right\}, \tag{4.21}$$

with respect to boundary conditions

$$f(0) = 0, \ f'(0) = \alpha^*, \ g(0) = 1, \ \theta(0) = 1, \ \phi(0) = 1, \ \xi(0) = 1 \ \text{at} \ \eta = 0$$

$$f' \to 0, \ g \to 0, \ \theta \to 0, \ \phi \to 0, \ \xi \to 0 \ \text{as} \ \eta \to \infty. \tag{4.22}$$

Now surface drag force, temperature gradient and Sherwood number can be define as

$$C_{f_r} = \frac{-2\tau_{w,r}}{\rho(u_w)^2}, \ C_{f_\vartheta} = \frac{-2\tau_{w,\vartheta}}{\rho(v_w)^2},$$

$$Nu_r = \frac{hq_w}{k(T_w - T_\infty)}, \ Sh_r = \frac{hJ_w}{D_B(C_w - C_\infty)}, \tag{4.23}$$

where shear stresses $\tau_{w,r}$, $\tau_{w,\vartheta}$ mass flux J_w and heat flux q_w are given by

$$\tau_{w,r} = (\tau_{zr})_{z=0} = \left(\mu \frac{\partial u}{\partial z}\right)_{z=0}, \ \tau_{w,\vartheta} = (\tau\vartheta)_{z=0} = \left(\mu \frac{\partial v}{\partial z}\right)_{z=0}$$

$$J_w = -k\left(\frac{\partial T}{\partial z}\right)_{z=0}, \ q_w - D_B\left(\frac{\partial C}{\partial z}\right)_{z=0}. \tag{4.24}$$

After substitiution values, we get

$$C_{f_r} = \frac{-2}{(\text{Re}_r)A^2}\left[1 - 2n\epsilon^2(f'(0))^2\right]f''(0),$$

$$C_{f_\vartheta} = \frac{-2}{(\text{Re}_r)}\left[1 - 2n\epsilon^2(f'(0))^2\right]g'(0),$$

$$Nu_r = -\theta'(0), \ Sh_r = -\phi'(0). \tag{4.25}$$

4.2 Results and discussion

Table 3 shows that surface drag force in radial and tangential direction is increased for higher estimation of Reynolds number Re and Hartmann number M while it decays for dimensionless constant n and material parameter ϵ_1. Table 3 demonstrates that surface drag force in tangential direction decays through heat transfer rate is affected by Brownian motion, Prandtl number, thermophoresis, Reynolds number and Schmidt and

43

Sherwood numbers are calculated in Table 4. It is observed that the heat transfer co-efficient increases with increasing values of the Brownian parameter, Prandtl number, Reynolds number, Schmidt number, whereas it decreases with rising values of the thermophoresis parameter, while Sherwood number is increased and becomes smaller with increasing levels of the Brownian parameter, thermophoresis parameter, Schmidt number, and Reynolds number. Figures 4.2(a-c) and 4.3(a-c) domonstrate a decrease in velocity profile when dimensionless constant N and material parameter ϵ_1 increased. Figures 4.4(a-b) shows the axial and radial velocities are rising with increasing α^*. It results from a rise in the stretching rate. Figure 4.4(c) show tangential velocity decays for larger α^*. Physically when the radial velocity profile f' asymptotically disappears in the absence of slip having arrived its greatest number and beginning beyond the border layer, starting at zero. It may be observed that the slip effect becomes stronger as velocity approaches closer to the wall. A drop in the azimuthal velocity component results from increasing the wall slip value. The disk's rotational impact, which is partially transmitted in the neighboring fluid layers, is what causes the azimuthal velocity component to decrease. In contrast to the velocity profiles, the temperature and concentration profiles seem to drop with increasing wall slip parameter values, also microorganism profile drop for higher values of slip parameter. Here's how something is explained. Figures 4.4(a-e) demonstrate a decrease in liquid temperature and concentration in the limit layer occurs when wall slip parameters are increased because the less (cold) liquid is pushed towards the crucial direction. Figures 4.5(a-c) depict the behavior of f, f' and g as the value of the Hall current parameter β_i changes. It is obvious from figures 4.5(a-c) that increasing the Hall current parameter β_i decreases the radial velocity f, tangential velocity f' and axial velocity g. In general, the influence of the Hall parameter β_i on the flow and thermal fields is more noticeable than that of the Ion-slip parameter β_e. Physically this is because the diffusion velocity of electrons is substantially greater than that of ions. Figures 4.6(a-d) illustrate the f, f', g, θ and ϕ profiles for various values of β_e ranging from 0.1 to 2.0. We see that when the Hall current parameter β_e grows, the radial velocity f, tangential

velocity f' axial velocity g and temperature θ increase while the concentration ϕ drops, because magnetic damping on f, f' and g reduces, and the magnetic field has a propulsive impact on f, f' and g. Figures 4.7(a-c) exhibit typical patterns for the fluid radial velocity f, tangential velocity f' axial velocity g, and temperature for various magnetic parameter M values. Increase in M values tend to impede the velocity of the fluid in the radial f and tangential f' directions while axial direction velocity g increases due to the damping effect of the magnetic field. When the Lewis number is increased, as seen in Figure 4.8(a), the microorganism profile is reduced concertation is reduced. Physically, a high Lewis number correlates to a reduced mass diffusivity, and hence a lower species concentration in nanofluid. But when the bioconvective parameter has increased the behavior of microorganisms is also increased, as seen in Figure 4.8(b). Figure 4.8(c), shows the reduction in microbe density and related boundary layer thickness caused by higher values of Pe. Higher values of Pe speed up cell swimming, which reduces the density of microorganisms. Figure 4.9(a) displays how the mass relaxation parameter λ_e affects the concentration profile. Concentration is increasing as the mass relaxation parameter is increased. Figures 4.9(b-d) show the effect of the concentration relaxation parameter λ_c on the temperature, concentration and microorganism profiles sketch ξ. Also shows the increase in temperature when the concentration relaxation parameter λ_c is given greater input values. It is because the modified Fick law is transformed into the original Fick law, demonstrating how mass instantly moves throughout the material as the fluid concentration increases.

Figures 4.10(a-d) show the effect of Buongiorno's model parameters (due to thermophoresis and Brownian motion) on the temperature and concentration field is seen. The thermophoretic force causes the temperature and concentration layer to shift from the lower to the upper area. Similarly, faster random mobility of species particles in nanofluids increased Brownian forces, which increased the temperature and concentration layer.

The proportion of momentum to mass diffusivities is known as the Schmidt number.

As can be observed from Figures 4.11(a-c), the reduction in ϕ, θ and ξ as Sc increases is caused by the decreased molecule diffusivity. Figures 4.11(a-c) illustrate how Sc has a diminishing effect on concentration. In terms of physics, a rise in Sc results in a decrease in molecule diffusivity, which raises the concentration. Prandtl number is the momentum-to-thermal diffusivity ratio. As a result, increasing Prandtl number results in lower thermal and concentration fields and as a result, an earlier convergence of the profile (see Figures 4.12).

Table 3: Numerical simulation for $C_{f_r}\mathrm{Re}_r$ and $C_{f_\vartheta}\mathrm{Re}_r$.

n	ϵ	M	$C_{f_r}\mathrm{Re}_r$	$C_{f_\vartheta}\mathrm{Re}_r$
0	0.1	0.2	1.47849	1.68799
1			1.42442	1.61457
2			1.36740	1.53947
	0.1		1.36740	1.53947
	0.2		1.24618	1.38717
	0.3		1.08798	1.25098
		0.2	1.36738	1.53947
		0.3	1.44775	1.58337
		0.4	1.52571	1.62643

Table 4: Numerical simulation for Nu_r and Sh_r.

Nb	Nt	Pr	Sc	Nu_r	Sh_r
0.3	0.4	1.5	0.1	0.465969	0.01814961
0.4				0.492788	0.07058772
0.5				0.528592	0.10280501
	0.4			0.465967	0.01814962
	0.5			0.408977	0.02999605
	0.6			0.359574	0.06258003
		1.5		0.465969	0.01814963
		1.6		0.474062	0.00920519
		1.7		0.408977	0.00181410
			0.1	0.465969	0.01814962
			0.2	0.496377	0.12774801
			0.3	0.521208	0.22708105
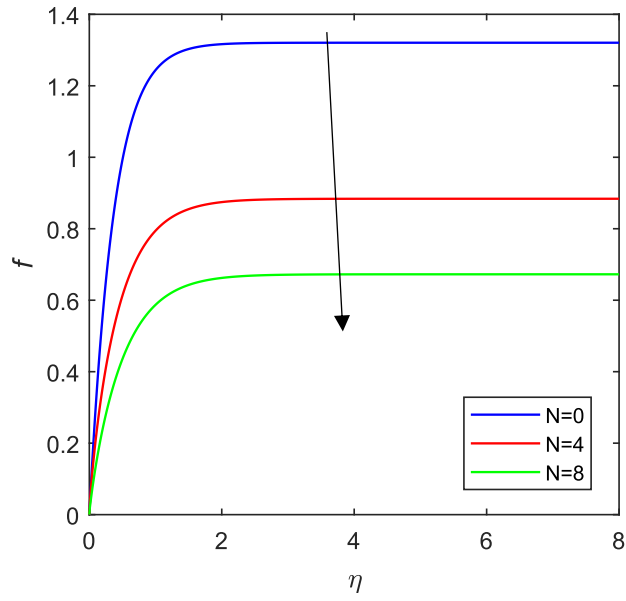
Figure 4.2(a) Plot of f against N.
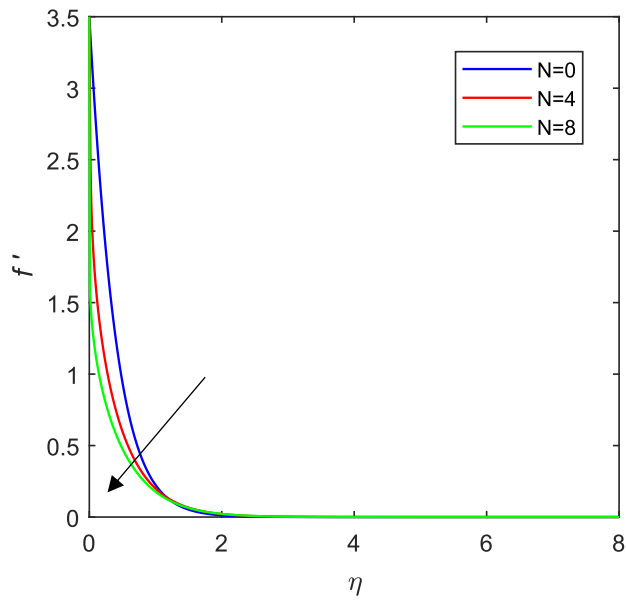
Figure 4.2(b) The plot of f' against N.
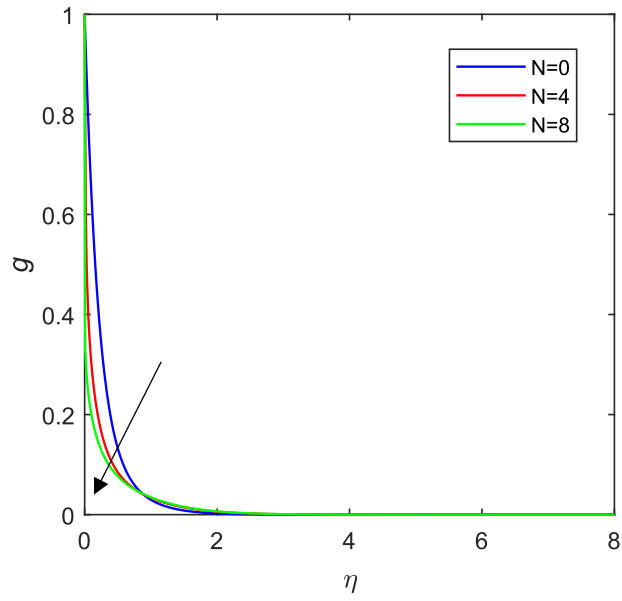
Figure 4.2(c) Plot of *g* against N.
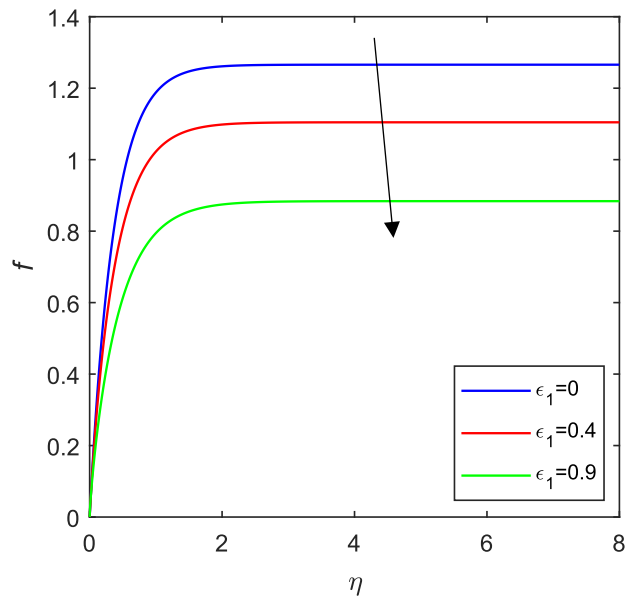
Figure 4.3(a) The plot of *f* against material parameter.
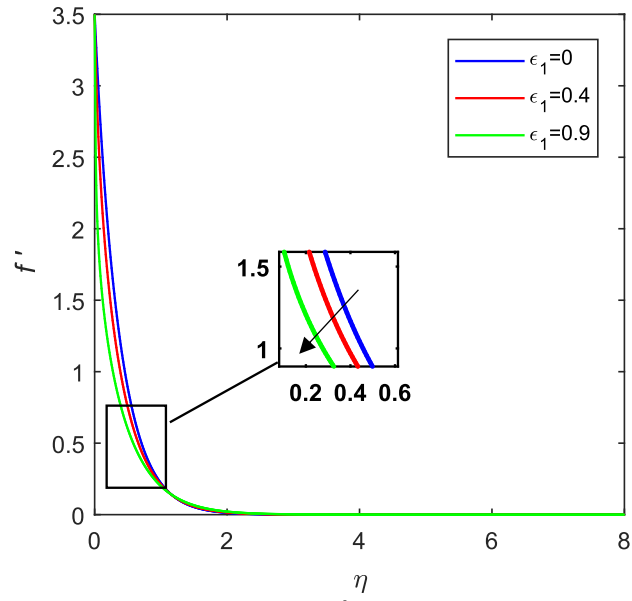
Figure 4.3(b) The plot of f' against material parameter.
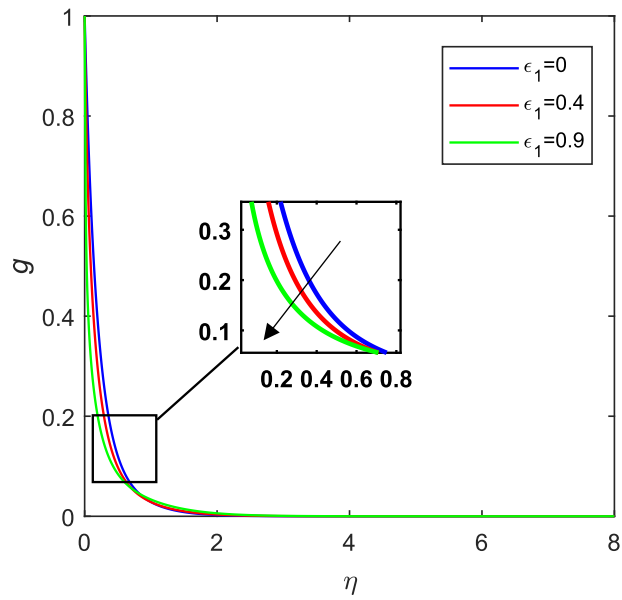
Figure 4.3(c) The plot of g against material parameter.
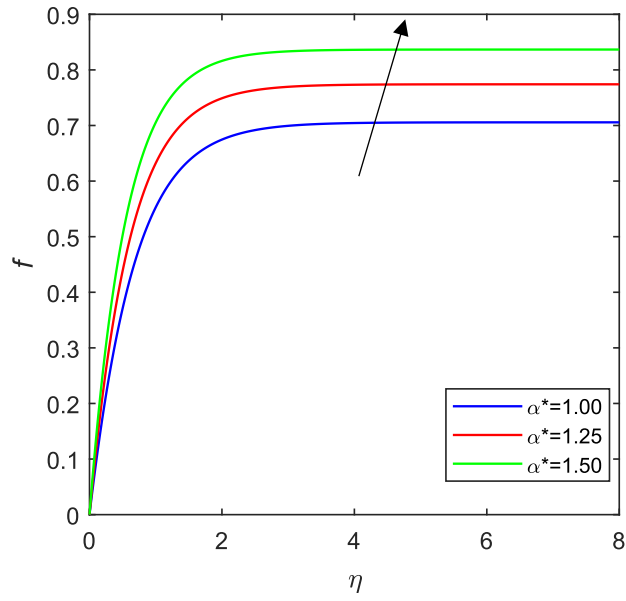
Figure 4.4(a) Plot of f against slip parameter.
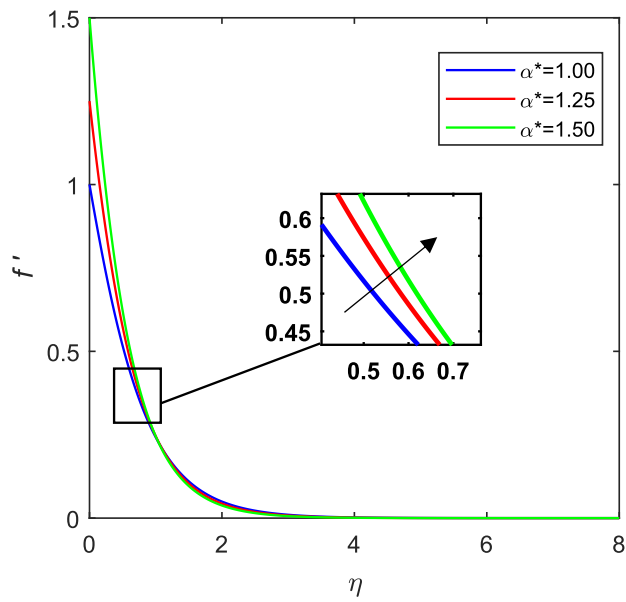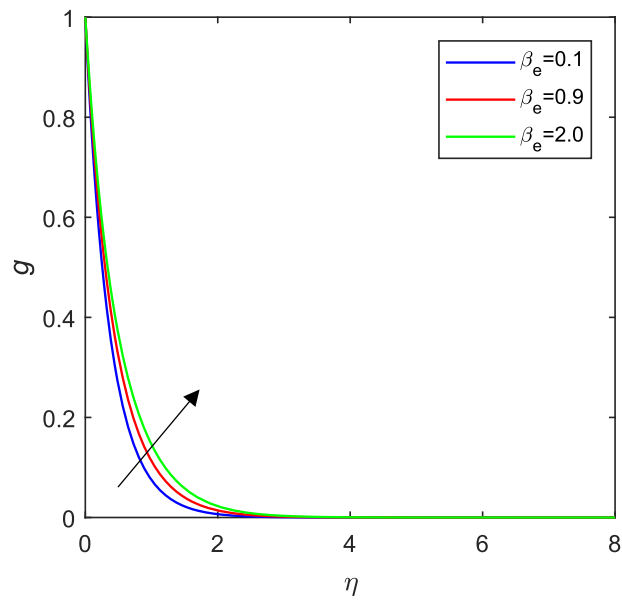

Figure 4.4(b) The plot of f' against slip parameter.
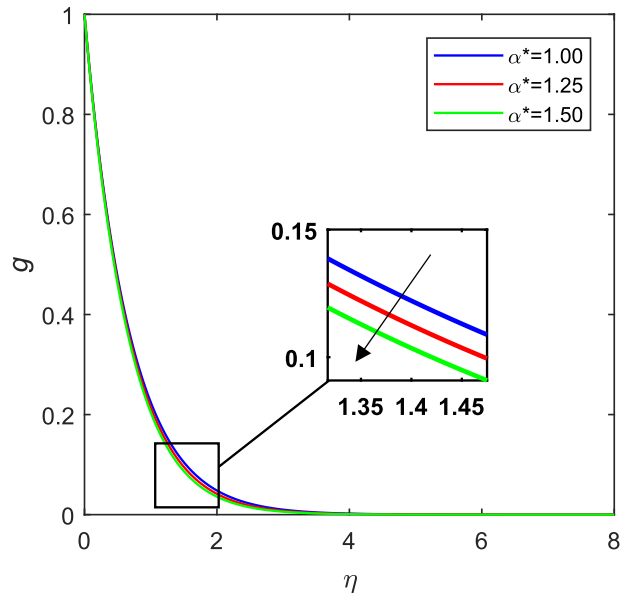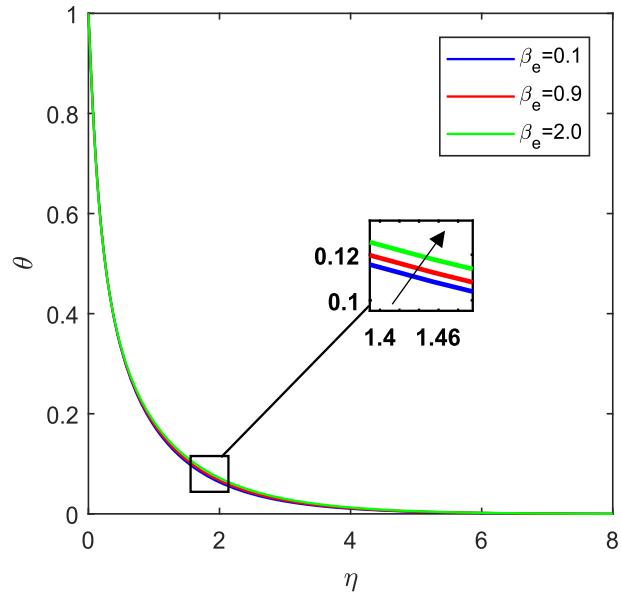
Figure 4.4(c) Plot of g against slip parameter.
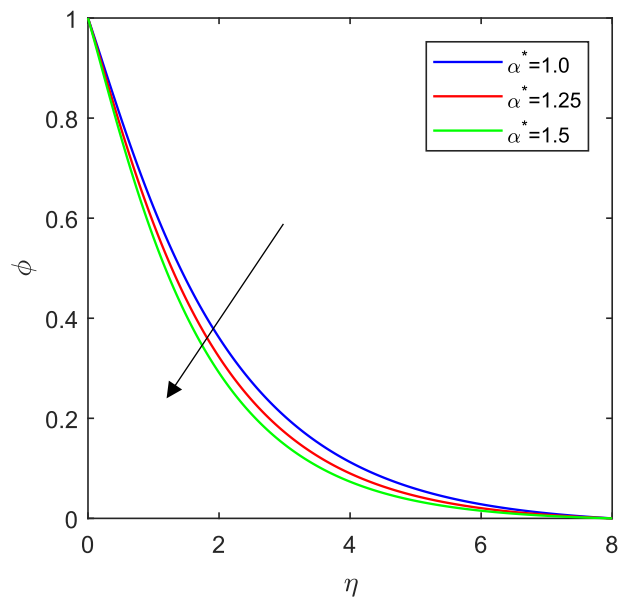
Figure 4.4(d) Plot of concentration against slip parameter.
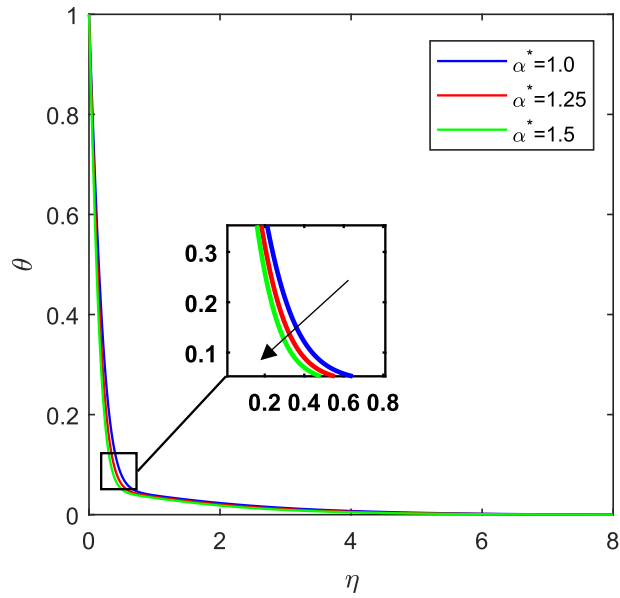
Figure 4.4(e) Plot of temperature against slip parameter.
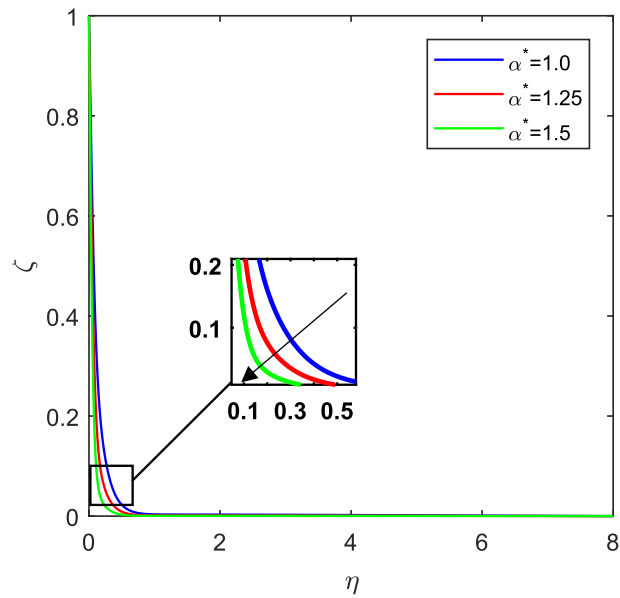
Figure 4.4(f) Plot of microorganism profile against slip parameter.
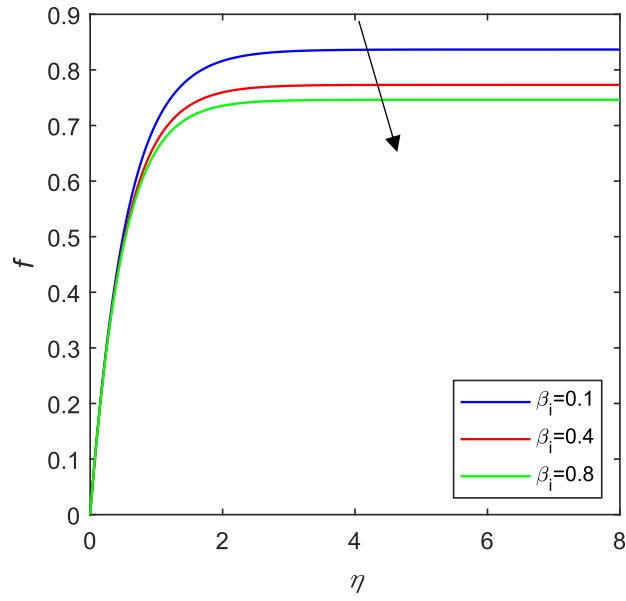
Figure 4.5(a) Plot of f against Hall current parameter.
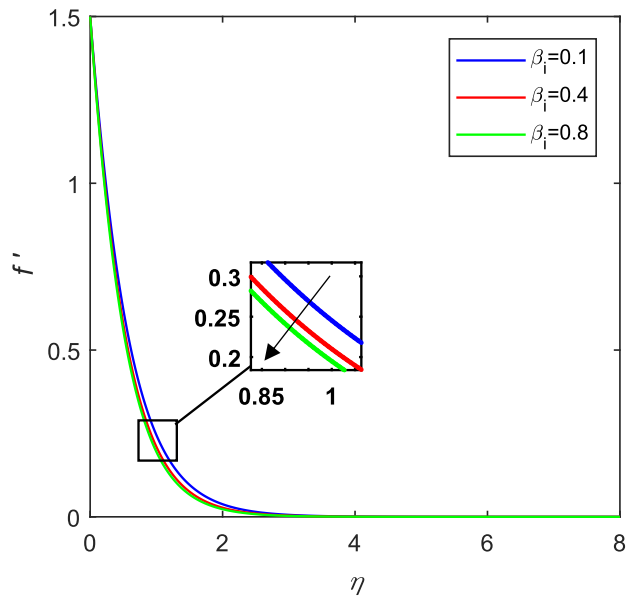
Figure 4.5(b) Plot of f' against Hall current parameter.
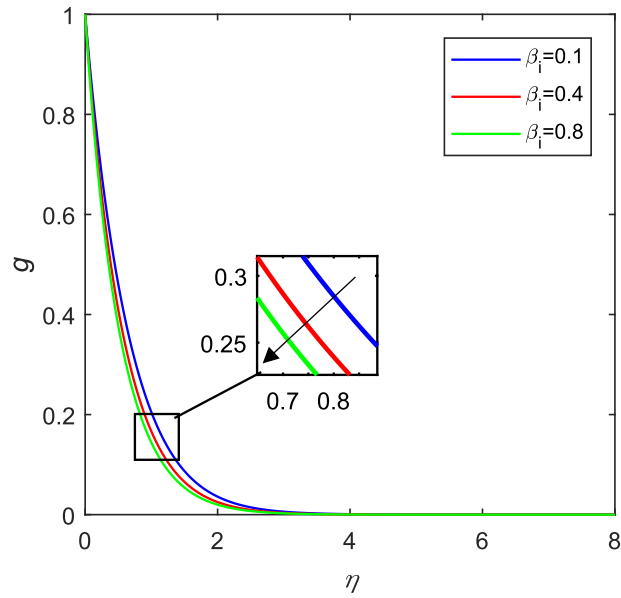
Figure 4.5(c) Plot of g against Hall current parameter.
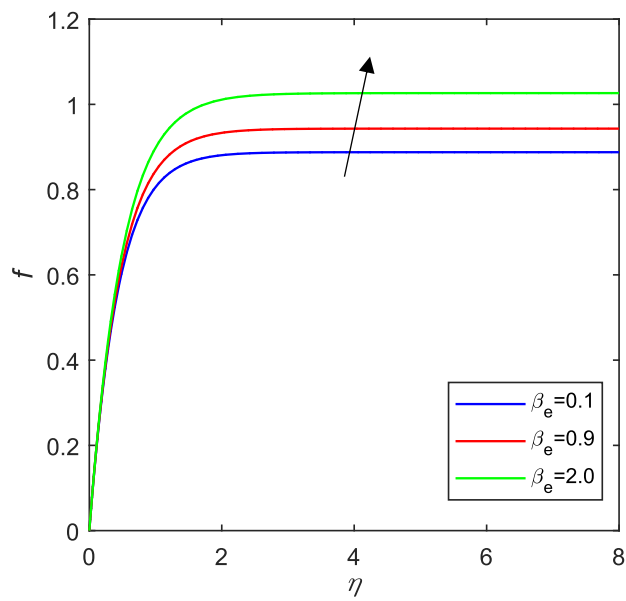
Figure 4.6(a) Plot of f against Ion slip parameter.
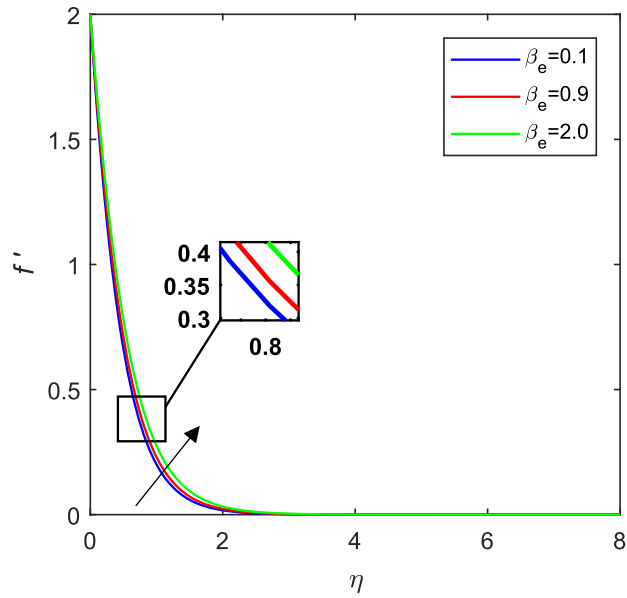
Figure 4.6(b) Plot of f' against Ion slip parameter.

Figure 4.6(c) Plot of g against Ion slip parameter.

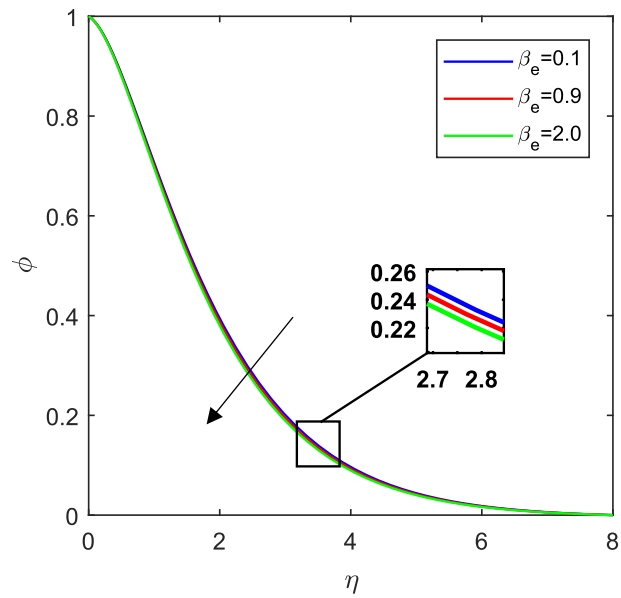Figure 4.6(d Plot of temperature against Ion slip parameter.

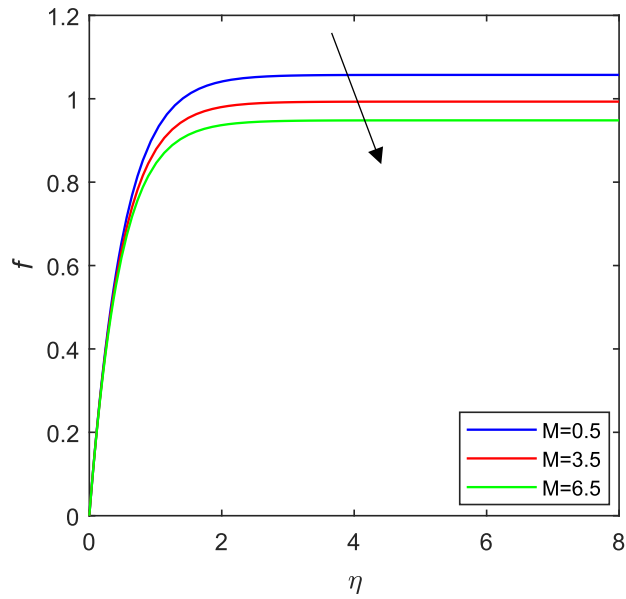Figure 4.6(e) Plot of concentration against Ion slip parameter.

57

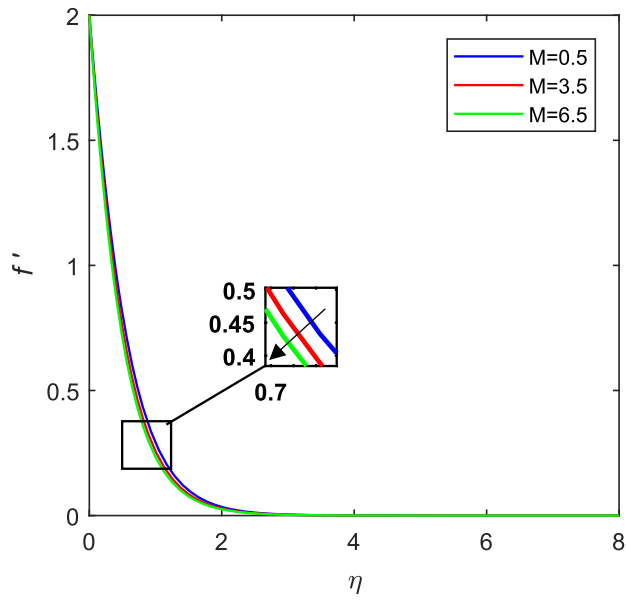Figure 4.7(a) Plot of f against Magnetic parameter.

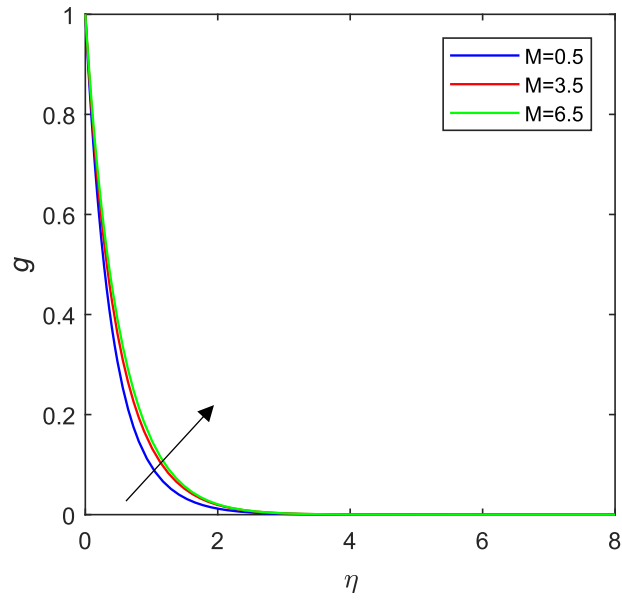Figure 4.7(b) Plot of f' against Magnetic parameter.

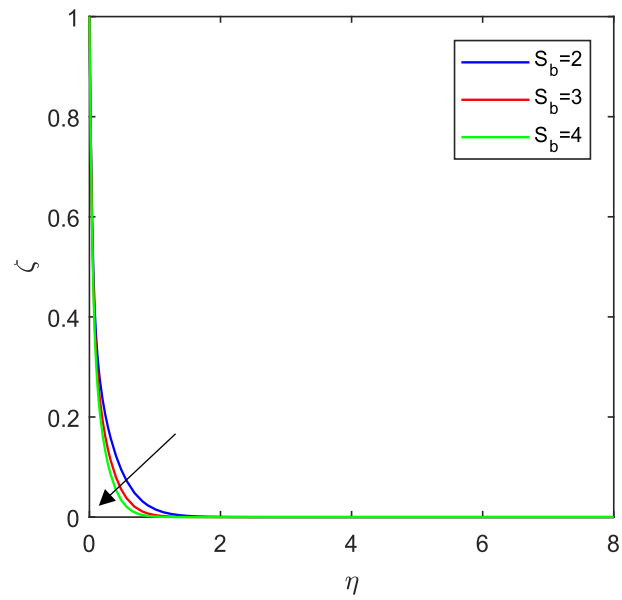Figure 4.7(c) Plot of g against Magnetic parameter.

Figure 4.8(a) Plot of microorganism profile against Bioconvective Lewis parameter.
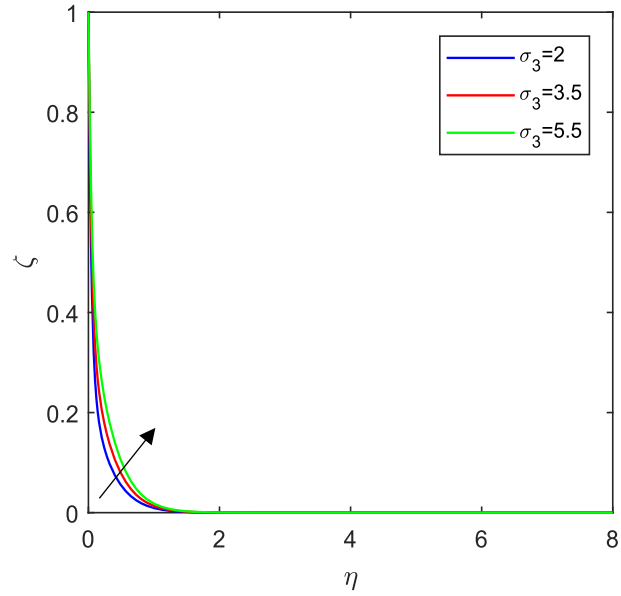
59

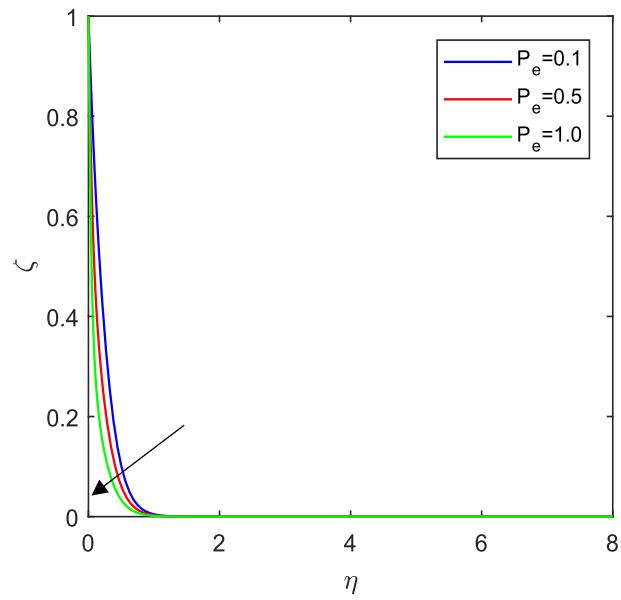Figure 4.8(b) Plot of zeta against Bio convective parameter.

Figure 4.8(c) Plot of zeta against Bioconvection Péclet number.
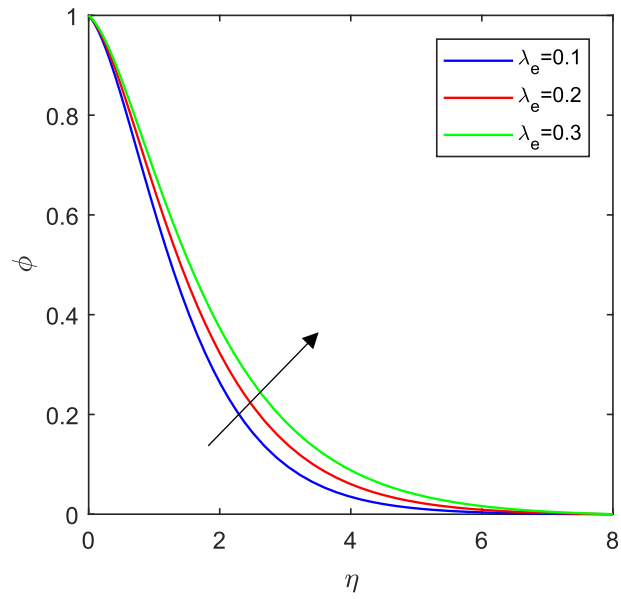
Figure 4.9(a) Plot of concentration against mass diffusion relaxation stress.
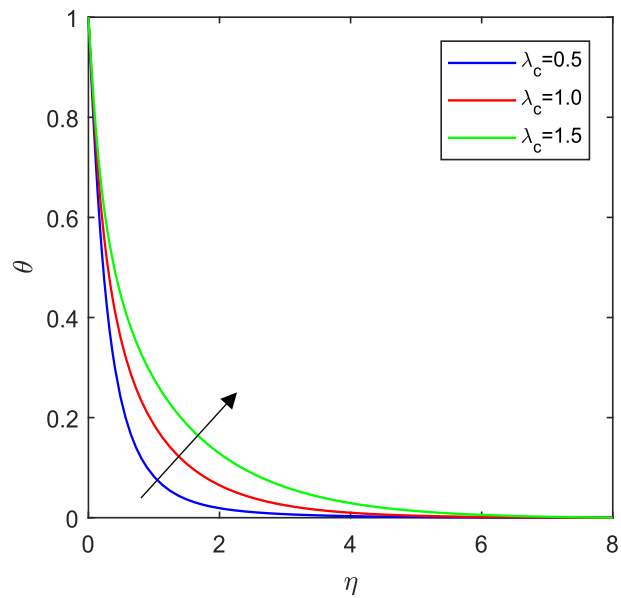
Figure 4.9(b) Plot of temperature profile against energy diffusion relaxation stress.
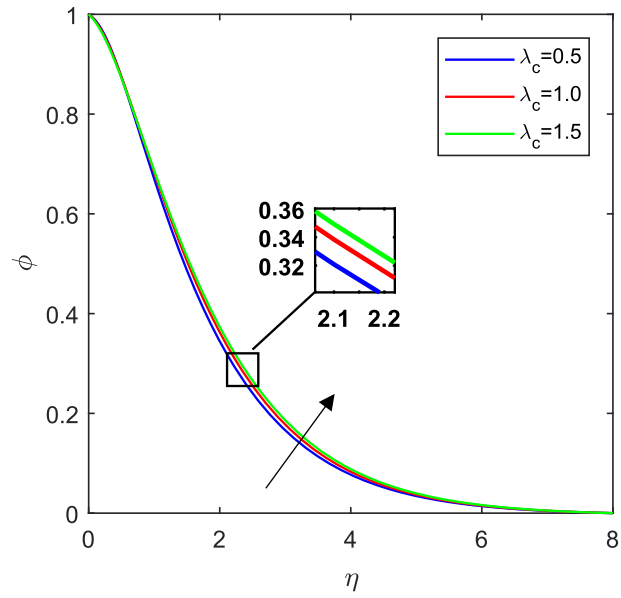
Figure 4.9(c). Plot of concertation against energy diffusion relaxation stress.
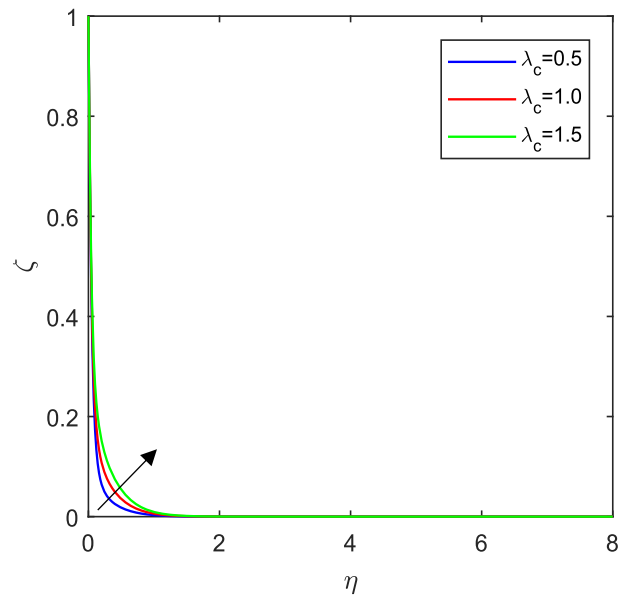
Figure 4.9(d) Plot of microorganism profile against energy diffusion relaxation stress.
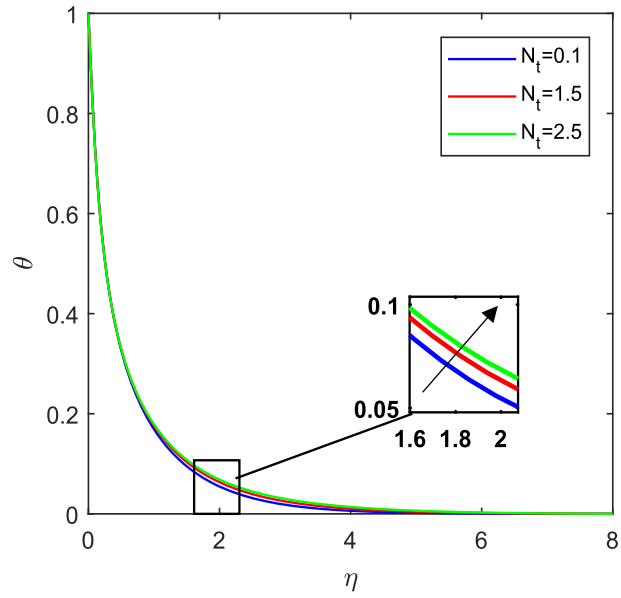
Figure 4.10(a) Plot of temperature profile against thermophoresis parameter.
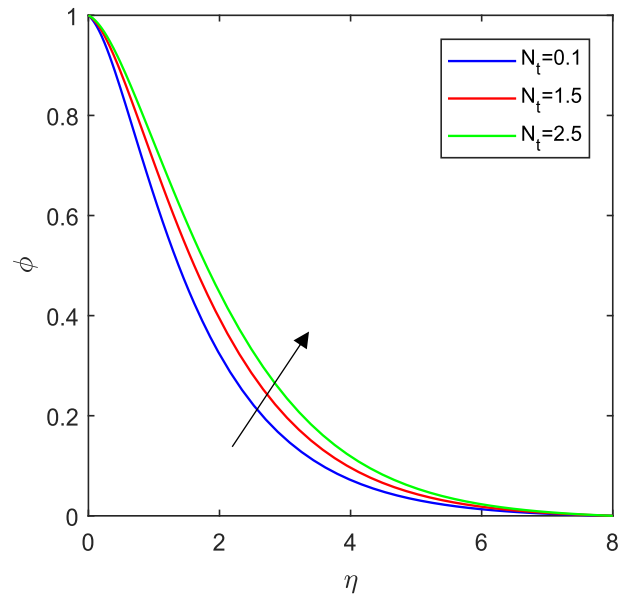
Figure 4.10(b) Plot of concentration against thermophoresis parameter.

63
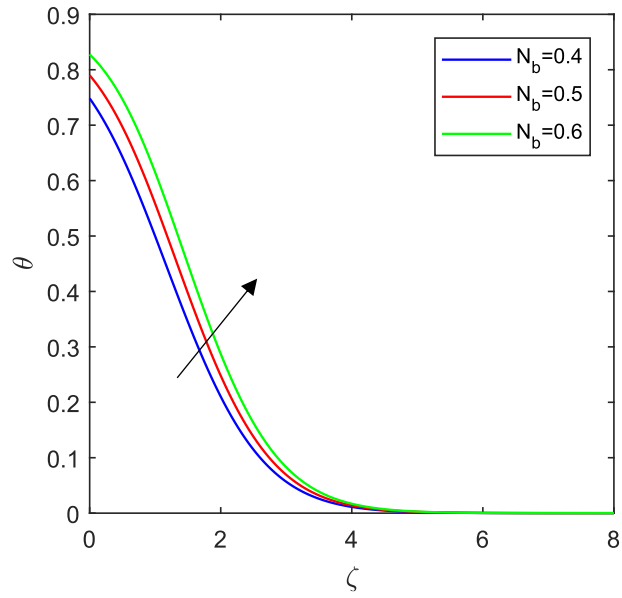
Figure 4.10(c). Plot of temperature against N_b Brownian motion parameter.
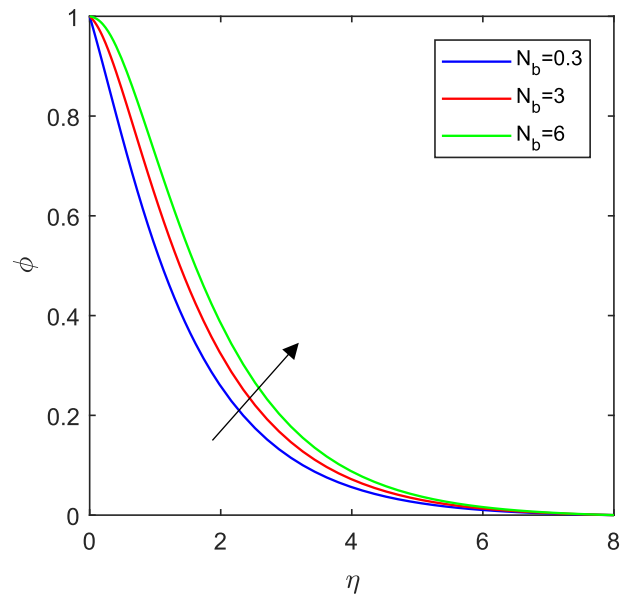
Figure 4.10(d) Plot of concentration against N_b Brownian motion parameter.
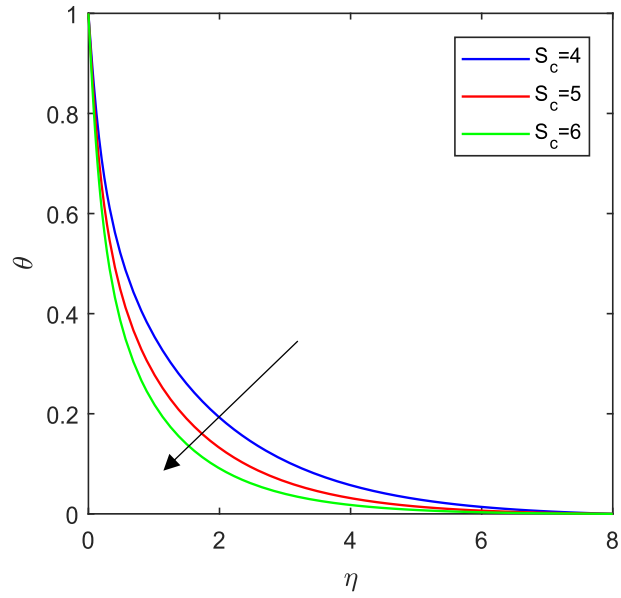
Figure 4.11(a) Plot of temperature profile against S_c Schmidt number.
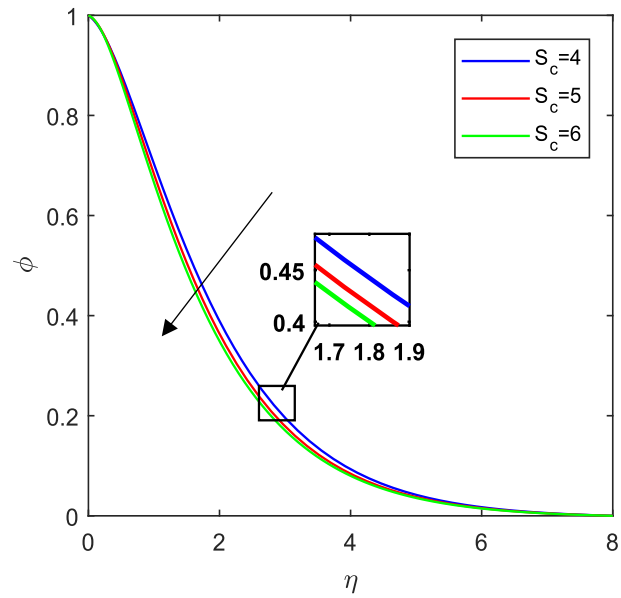
Figure 4.11(b) Plot of concentration against S_c Schmidt number.
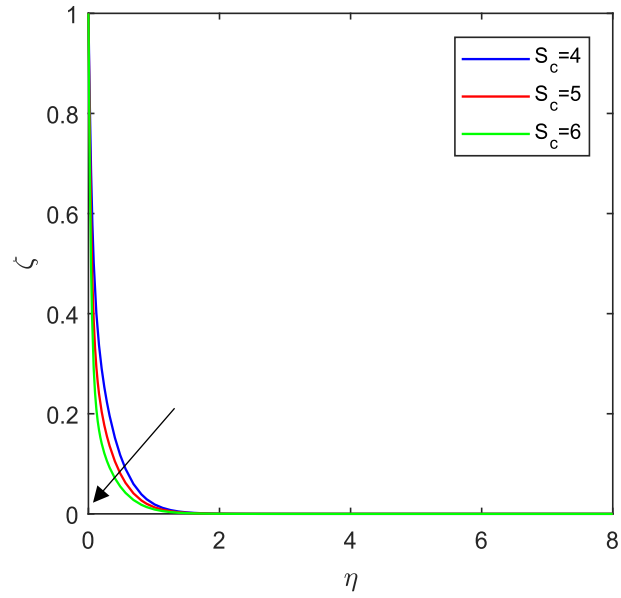
Figure 4.11(c) Plot of microorganism against S_c Schmidt number.
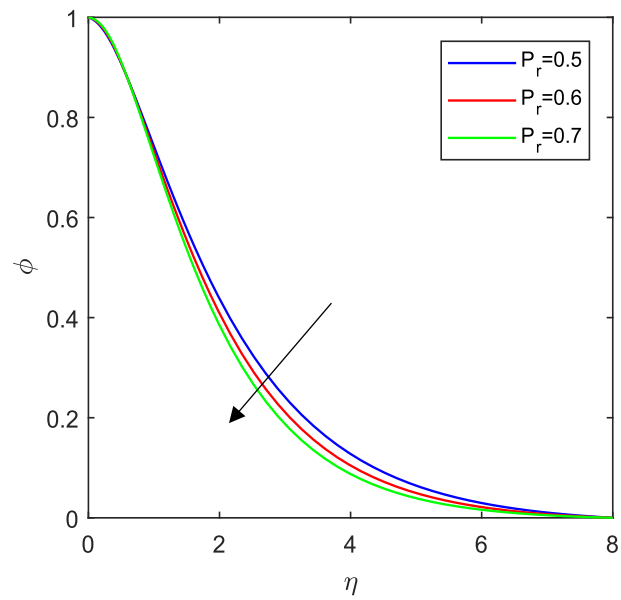
Figure 4.12 Plot of concentration against P_r Prandtl number.

Chapter 5

Conclusion

5.1 Conclusions (Chapter 3)

We may write the following major points based on the analysis of chapter 3:

- A decrease in radially outward flow is caused by a rise in the fluid parameter.

- As skin friction and driving torque are decreased, higher viscoelastic effects are evident.

- Increase in wall roughness parameter increase resisting torque and skin friction, whereas entrainment velocity has the reverse effect.

- The radial velocity profile decreases as the wall roughness parameter increases.

- Temperature profiles rise and concentrations increase as a result of the Reiner-Rivlin fluid parameter, wall roughness, and thermophoretic parameter, whereas the Brownian motion parameter causes these profiles to drop.

- The rate of heat transmission increases with higher values of the Schmidt number, Brownian motion, thermophoretic, and thermal slip parameters.

- The Reiner-Rivlin, thermophoretic, and thermal slip parameters grow as the local Nusselt and Sherwood numbers increase.

5.2 Conclusions (Chapter 4)

The key observations of chapter 4 are as under:

- Drop in velocity profile when dimensionless constant and material parameter increased.
- A decrease in velocity profile is caused by a rise in the slip parameter.
- Increase in Hall current parameters decreasing velocity profiles.
- Increase in Ion slip parameters cause increase in velocity profiles as well as temperature profile.
- A decrease in velocity profile while are increase in azimuthal velocity are caused by strong Magnetic field.
- A drop in microorganism profile when rise in bioconvective Lewis parameter and Bioconvection Péclet number, while microorganism profile is rise when Bio convective parameter increases.
- Rise in concentration profile when increase in mass diffusion parameter.
- Rise in temperature, concertation and microorganism profiles when increase in energy diffusion relaxation parameter.
- Increse in temperature and concentration profiles when rise in thermophoresis and Brownian motion parameter.
- Drop in temperature, concentration and microorganism profiles is observed when increase in Schmidt number.
- Drop in concentration profile is observed for different values of Prandtl number.
- Sherwood number boosts with increasing levels of the Brownian parameter.

Bibliography

[1] Choi, S. U., & Eastman, J. A. Enhancing thermal conductivity of fluids with nanoparticles Argonne National Lab.(ANL), Argonne, IL (United States). No. ANL/MSD/CP-84938, CONF-951135-29, 1995.

[2] Feteca C, Vieru D, Azhar WA. Natural convection flow of fractional nanofluid sover an isothermal vertical plate with thermal radiation. Applied Sciences, pp. 7:247, 2017.

[3] Bhatti, M. M., & Rashidi, M. M. Effects of thermo-diffusion and thermal radiation on Williamson nanofluid over a porous shrinking/stretching sheet. Journal of Molecular Liquids, 221, pp. 567-573, 2016.

[4] Turkyilmazoglu, M. Flow of nanofluid plane wall jet and heat transfer. European Journal of Mechanics-B/Fluids, 59, pp. 18-24, 2016.

[5] Venthan, S. M., Amalraj, I. J., & Kumar, P. S.. Analysis of entrance region flow of Bingham nanofluid in concentric annuli with rotating inner cylinder. Micro & Nano Letters, 14(13), pp. 1361-1365, 2019.

[6] Waqas, H., Imran, M., Khan, S. U., Shehzad, S. A., & Meraj, M. A. Slip flow of Maxwell viscoelasticity-based micropolar nanoparticles with porous medium: a numerical study. Applied Mathematics and Mechanics, 40(9), pp. 1255-1268, 2019.

[7] Ali, M., Sultan, F., Khan, W. A., Shahzad, M., & Arif, H.. Important features of expanding/contracting cylinder for Cross magneto-nanofluid flow. Chaos, Solitons & Fractals, pp. 133, 109656 , 2020.

[8] Stokes, V. K. Couple stresses in fluids. In Theories of fluids with microstructure Springer, Berlin, Heidelberg. pp. 34-80, 1984.

[9] Stokes, V. K. Effects of couple stresses in fluids on hydromagnetic channel flows. The Physics of Fluids, 11(5), pp. 1131-1133, 1968.

[10] Van D'ep, Nguen Equations of a fluid boundary layer with couple stresses: Journal of Applied Mathematics and Mechanics, 32(4), pp. 777-783, 1968.

[11] Soundalgekar, V. M. Effects of couple stresses in fluids on dispersion of a solute in a channel flow. The Physics of Fluids, 14(1), pp. 19-20, 1971.

[12] Chaturani, P., & Upadhya, V. S.. Pulsatile flow of a couple stress fluid through circular tubes with applications to blood flow. Biorheology, 15(3-4), pp. 193-201, 1978.

[13] Sagayamary, R. V., & Devanathan, R. Steady flow of couple stress fluid through tubes of slowly varying cross-sections–Application to blood flows. Biorheology, 26(4), pp. 753-769, 1989.

[14] Hiremath, P. S., & Patil, P. M. Free convection effects on the oscillatory flow of a couple stress fluid through a porous medium. Acta Mechanica, 98(1), pp. 143-158, 1993.

[15] Jangili, S., Adesanya, S. O., Ogunseye, H. A., & Lebelo, R. Couple stress fluid flow with variable properties: a second law analysis. Mathematical Methods in the Applied Sciences, 42(1), pp. 85-98, 2019.

[16] Adesanya, S. O., & Makinde, O. D. Entropy generation in couple stress fluid flow through porous channel with fluid slippage. International Journal of Exergy, 15(3), pp. 344-362, 2014.

[17] Ramzan, M., Farooq, M., Alsaedi, A., & Hayat, T. MHD three-dimensional flow of couple stress fluid with Newtonian heating. The European Physical Journal Plus, 128(5), pp. 1-15, 2013.

[18] Sutterby, J. L. Laminar converging flow of dilute polymer solutions in conical sections: Part I. Viscosity data, new viscosity model, tube flow solution. AIChE Journal, 12(1), pp. 63-68, 1966.

[19] Hayat, T., Bibi, F., Khan, A. A., & Alsaedi, A. Entropy production minimization and non-Darcy resistance within wavy motion of Sutterby liquid subject to variable physical characteristics. Journal of Thermal Analysis and Calorimetry, 143(3), pp. 2215-2225, 2021.

[20] Imran, N., Javed, M., Sohail, M., Thounthong, P., & Abdelmalek, Z. Theoretical exploration of thermal transportation with chemical reactions for sutterby fluid model obeying peristaltic mechanism. Journal of Materials Research and Technology, 9(4), pp. 7449-7459, 2020.

[21] Lin, P., & Ghaffari, A. Heat and mass transfer in a steady flow of Sutterby nanofluid over the surface of a stretching wedge. Physica Scripta, 96(6), pp. 065003, 2021.

[22] Hayat, T., Khan, A. A., Bibi, F., & Alsaedi, A. Entropy minimization for magneto peristaltic transport of Sutterby materials subject to temperature dependent thermal conductivity and non-linear thermal radiation. International Communications in Heat and Mass Transfer, 122, pp. 105009, 2021.

[23] Buongiorno J Convective transport in nanofluids. Journal of Heat Transfer 128(3): pp. 240–250, 2006.

[24] Karman, T. V. Z. angew. Math. u. Mechanik, pp. 233, 1921.

[25] Millsaps, K., & Pohlhausen, K. Heat transfer by laminar flow from a rotating plate. Journal of the Aeronautical Sciences, 19(2), pp. 120-126, 1952.

[26] Shevchuk, I. V., & Buschmann, M. H. Rotating disk heat transfer in a fluid swirling as a forced vortex. Heat and Mass Transfer, 41(12), pp. 1112-1121, 2005.

[27] Ramzan, M., Chung, J. D., & Ullah, N. Radiative magnetohydrodynamic nanofluid flow due to gyrotactic microorganisms with chemical reaction and non-linear thermal radiation. International Journal of Mechanical Sciences, 130, pp. 31-40, 2017.

[28] Kuznetsov, A. V., & Jiang, N. Bioconvection of negatively geotactic microorganisms in a porous medium: the effect of cell deposition and declogging. International Journal of Numerical Methods for Heat & Fluid Flow, 2003.

[29] Ghorai, S., & Hill, N. A. Wavelengths of gyrotactic plumes in bioconvection. Bulletin of Mathematical Biology, 62(3), pp. 429-450, 2000.

[30] Sharma, Y. D., & Kumar, V. The effect of high-frequency vertical vibration in a suspension of gyrotactic micro-organisms. Mechanics Research Communications, 44, pp. 40-46, 2012.

[31] Yanaoka, H., Inamura, T., & Suzuki, K. Numerical analysis of bioconvection generated by chemotactic bacteria. Journal of Fluid Science and Technology, 4(3), pp. 536-545, 2009.

[32] Grattan-Guinness, I. Joseph fourier, théorie analytique de la chaleur, In Landmark Writings in Western Mathematics Elsevier Science, pp. 354-365, 2005.

[33] Esfahani, J. A., & Bordbar, V. Double diffusive natural convection heat transfer enhancement in a square enclosure using nanofluids. Journal of Nanotechnology in Engineering and Medicine, 2(2), 2011.

[34] Zheng, L., Liu, Y., & Zhang, X. Slip effects on MHD flow of a generalized Oldroyd-B fluid with fractional derivative. Nonlinear Analysis: Real World Applications, 13(2), pp. 513-523, 2012.

[35] Sahoo, B., & Poncet, S. Flow and heat transfer of a third grade fluid past an exponentially stretching sheet with partial slip boundary condition. International Journal of Heat and Mass Transfer, 54(23-24), pp. 5010-5019, 2011.

[36] Han, S., Zheng, L., Li, C., & Zhang, X. Coupled flow and heat transfer in viscoelastic fluid with Cattaneo–Christov heat flux model. Applied Mathematics Letters, 38, pp. 87-93, 2014.

[37] Zheng, L., Zhang, C., Zhang, X., & Zhang, J. Flow and radiation heat transfer of a nanofluid over a stretching sheet with velocity slip and temperature jump in porous medium. Journal of the Franklin Institute, 350(5), pp. 990-1007, 2013.

[38] Javed, T., & Mustafa, I. Slip effects on a mixed convection flow of a third-grade fluid near the orthogonal stagnation point on a vertical surface. Journal of Applied Mechanics and Technical Physics, 57(3), pp. 527-536, 2016.

[39] Chauhan, D. S., & Olkha, A. Slip flow and heat transfer of a second-grade fluid in a porous medium over a stretching sheet with power-law surface temperature or heat flux. Chemical Engineering Communications, 198(9), pp. 1129-1145, 2011.

[40] Hina, S., Mustafa, M., Hayat, T., & Alsaedi, A.. Peristaltic flow of Powell-Eyring fluid in curved channel with heat transfer: A useful application in biomedicine. Computer Methods and Programs in Biomedicine, 135, pp. 89-100, 2016.

[41] Abbasbandy, S., Mustafa, M., Hayat, T., & Alsaedi, A.. Slip effects on MHD boundary layer flow of Oldroyd-B fluid past a stretching sheet: An analytic solution. Journal of the Brazilian Society of Mechanical Sciences and Engineering, 39(9), pp. 3389-3397, 2017.

[42] Prasad, K. V., Vajravelu, K., & Vaidya, H. Hall effect on MHD flow and heat transfer over a stretching sheet with variable thickness. International Journal for Computational Methods in Engineering Science and Mechanics, 17(4), pp. 288-297, 2016.

[43] Tani, I. Steady flow of conducting fluids in channels under transverse magnetic fields, with consideration of Hall effect. Journal of the Aerospace Sciences, 29(3), pp. 297-305, 1962.

[44] Hayat, T., Shafique, M., Tanveer, A., & Alsaedi, A. Hall and Ion slip effects on peristaltic flow of Jeffrey nanofluid with Joule heating. Journal of Magnetism and Magnetic Materials, 407, pp. 51-59. 2016.

[45] Srinivasacharya, D., & Shafeeurrahman, M. Hall and Ion slip effects on mixed convection flow of nanofluid between two concentric cylinders. Journal of the Association of Arab Universities for Basic and Applied Sciences, 24, pp. 223-231, 2017.

[46] Veera Krishna, M., & Chamkha, A. J. Hall effects on unsteady MHD flow of second grade fluid through porous medium with ramped wall temperature and ramped surface concentration. Physics of Fluids, 30(5), pp. 053101, 2018.

[47] Tlili, I., Hamadneh, N. N., Khan, W. A., & Atawneh, S. Thermodynamic analysis of MHD Couette–Poiseuille flow of water-based nanofluids in a rotating channel with radiation and Hall effects. Journal of Thermal Analysis and Calorimetry, 132(3), pp. 1899-1912, 2018.

[48] Abbasi, F. M., Gul, M., & Shehzad, S. A. Hall effects on peristalsis of boron nitride-ethylene glycol nanofluid with temperature dependent thermal conductivity. Physica E: Low-dimensional Systems and Nanostructures, 99, pp. 275-284, 2018.

[49] Su, X. Hall and Ion-slip effects on the unsteady MHD mixed convection of Cu-water nanofluid over a vertical stretching plate with convective heat flux. Indian Journal Pure Applied Physics, pp. 53, 2015, pp. 643, 2017.

[50] Bilal, M., Hussain, S., & Sagheer, M. Boundary layer flow of magneto-micropolar nanofluid flow with Hall and Ion-slip effects using variable thermal diffusivity. Bulletin of the Polish Academy of Sciences. Technical Sciences, pp. 65(3), 2017.

[51] Sha, Z., Dawar, A., Alzahrani, E. O., Kumam, P., Khan, A. J., & Islam, S. Hall effect on couple stress 3D nanofluid flow over an exponentially stretched surface with Cattaneo Christov heat flux model. IEEE Access, 7, pp. 64844-64855, 2019.

[52] Shah, Z., Islam, S., Gul, T., Bonyah, E., & Khan, M. A. The electrical MHD and hall current impact on micropolar nanofluid flow between rotating parallel plates. Results in Physics, 9, pp. 1201-1214, 2018.

[53] Tabassum, M., & Mustafa, M. A numerical treatment for partial slip flow and heat transfer of non-Newtonian Reiner-Rivlin fluid due to rotating disk. International Journal of Heat and Mass Transfer, 123, pp. 979-987, 2018.

[54] Christov, C. I. On frame indifferent formulation of the Maxwell–Cattaneo model of finite-speed heat conduction. Mechanics Research Communications, 36(4), pp. 481-486, 2009.

[55] Bonisoli, A. Atti del Seminario Matematico e Fisico dell'Università di Modena e Reggio Emilia, vol. 53, fasc. 2, 2005.

[56] Reiner, M. A mathematical theory of dilatancy. American Journal of Mathematics, 67(3), pp. 350-362, 1945.

[57] Rivlin, R. S. Hydrodynamics of non-Newtonian fluids. Nature, 160(4070), pp. 611-611, 1947.

[58] Tabassum, M., & Mustafa, M. A numerical treatment for partial slip flow and heat transfer of non-Newtonian Reiner-Rivlin fluid due to rotating disk. International Journal of Heat and Mass Transfer, 123, pp. 979-987, 2018.

thesis asad

16%	**6**%	**13**%	**4**%
SIMILARITY INDEX	INTERNET SOURCES	PUBLICATIONS	STUDENT PAPERS

PRIMARY SOURCES

1   Submitted to Higher Education Commission Pakistan
Student Paper   **3**%

2   Syed Muhammad Raza Shah Naqvi, Hyun Min Kim, Taseer Muhammad, Fouad Mallawi, Malik Zaka Ullah. "Numerical study for slip flow of Reiner-Rivlin nanofluid due to a rotating disk", International Communications in Heat and Mass Transfer, 2020
Publication   **2**%

3   coek.info
Internet Source   **1**%

4   Osalusi, E.. "The effects of Ohmic heating and viscous dissipation on unsteady MHD and slip flow over a porous rotating disk with variable properties in the presence of Hall and ion-slip currents", International Communications in Heat and Mass Transfer, 200711
Publication   **1**%

5   Basant K. Jha, Gabriel Samaila, Peter B. Malgwi. "Adomian decomposition method for   **<1**%